Effective Macroscopic Equations for Biological Fluid and Nutrients' Transport in Vascularized Tumors Growing Via Proliferation and Chemotaxis

Mathematical Methods in the Applied Sciences

WILEY

RESEARCH ARTICLE OPEN ACCESS

Effective Macroscopic Equations for Biological Fluid and Nutrients' Transport in Vascularized Tumors Growing Via Proliferation and Chemotaxis

Francesca Ballatore[1] | Chiara Giverso[1] | Raimondo Penta[2]

[1]Department of Mathematical Sciences "G.L. Lagrange", Politecnico di Torino, Torino, Italy | [2]School of Mathematics and Statistics, University of Glasgow, Glasgow, UK

Correspondence: Raimondo Penta (Raimondo.Penta@glasgow.ac.uk)

Received: 19 November 2024 | **Revised:** 14 May 2025 | **Accepted:** 16 May 2025

Funding: F.B, C.G., and R.P. conducted the research according to the inspiring scientific principles of the National Italian Mathematics Association Indam ("Istituto nazionale di Alta Matematica"), GNFM group. R.P. is partially supported by EPSRC, UK grants EP/S030875/1 and EP/T017899/1. F.B. acknowledges support from the PNRR M4C2 through the project "Made in Italy Circolare e Sostenibile (MICS)," CUP: E13C22001900001.

Keywords: asymptotic homogenization | chemotactic flux | double porosity model | tumor growth modeling | vascularised materials

ABSTRACT

This paper presents a system of partial differential equations designed to model fluid and nutrient transport within the growing tumor microenvironment. The fluid phase, representing both cells and extracellular fluids flowing within the interstitial space, is assumed to be intrinsically incompressible, so that growth can be modeled as a source, generally defined by volumetric growth terms and nonconvective mass fluxes. Specifically, we consider the volumetric growth term proportional to the nutrient concentration and the nonconvective mass flux driven by the nutrient gradient. By exploiting the scale separation between the microscopic vascular structures and the larger tumor tissue, we employ asymptotic homogenization to derive effective macroscopic equations that integrate detailed microscale characteristics. The resulting model operates as a double porous medium framework, where fluid dynamics are driven by both pressure and concentration gradient, which reduces to a more standard Darcy's law when microscale variations of the convective mass flux are neglected. Nutrient transport is captured through a coupled advection–diffusion–reaction system. Permeability and diffusivity tensors, which encapsulate the influence of microvascular geometry, are computed via cell-problem analysis to accurately reflect the microscale structure within the macroscopic model. Given that the tissue model includes a fluid phase that continually exchanges with the surrounding vasculature, along with nutrients, the Kedem–Katchalsky formulation is employed to represent fluid and nutrient transport across the capillary walls. This approach provides valuable insights into the interactions between vascular architecture and tumor growth. Although certain limitations remain, such as the static tumor domain and assumptions regarding cell proliferation, the framework offers a foundation for further development. It is adaptable for numerical simulations based on real tumor geometries, with promising potential to inform and improve anticancer treatment strategies through the integration of patient-specific clinical data.

1 | Introduction

Asymptotic homogenization is a widely used upscaling technique designed to analyze and model multiscale systems, where phenomena manifest across different scales, see, for example, [1–3], on classic, formal, homogenization for composites, as well as [4] on more rigorous aspects concerning the two-scale convergence.

By exploiting the separation of scales, asymptotic homogenization enables a systematic transition from detailed microscopic descriptions to simplified macroscopic models, while preserving essential microscale information encapsulated in effective parameters at a reduced computational cost [5]. The method involves expanding the system's variables in terms of a small parameter that represents the ratio between microscopic and macroscopic scales. Through this expansion, a hierarchy of equations emerges, describing the system's behavior at different scales. Homogenizing these equations allows for the derivation of effective properties and governing equations at the macroscopic level. These effective equations typically include parameters that reflect the influence of the underlying microscale structures, thus bridging the gap between intricate microscale behavior and observable macroscale phenomena.

The multiple scales method has proven to be highly effective in a wide range of physical systems, particularly in the analysis of composite materials [6–10], as well as porous media flow [11]. These systems normally exhibit different hierarchical levels of organization related to different, typically increasingly larger length scales associated, for example, with the size of the pores, distance between individual branches of interconnected networks, and size of the overall domain.

Relevant application of the asymptotic homogenization technique to hierarchical porous materials includes, for example, geomaterials [12, 13], which can, for instance, play a role in the drainage of disposed liquid, oil and gas extraction, consolidation, as well as glaciers and aquifers dynamics, industrial applications, such as filters' optimization [14] as well as biological and bio-inspired tissues. The latter include, but are not limited to, bone and tendons [15], implants [16], and organs, such as the brain [17], the heart [18], the lymphatic system [19, 20], as well as healthy [21] and malignant cell aggregates, for example, avascular [22, 23] and vascular tumors [24–26]. Moreover, we acknowledge that microstructural evolution within the framework of asymptotic homogenization has been explored in both biological and industrial contexts. For instance, it has been applied to describe heterogeneous tissue dynamics [27], flow through filters with porosity gradients [28], and appositional growth in additive manufacturing [29], highlighting the broad applicability and versatility of such multiscale techniques.

The modeling framework developed in tumor studies proves particularly valuable for analyzing the complex interplay between tumor growth and the transport of drugs and nutrients within the surrounding capillary network [30]. Tumors depend on blood vessels to supply essential nutrients and oxygen, a process driven by angiogenesis [31]. However, the vasculature formed through angiogenesis is often irregular and heterogeneous, resulting in spatial variations in fluid flow and nutrient distribution. Understanding the dynamics of flow and chemical exchange between this complex vasculature and the tissue and its impact on tumor growth is critical for deepening our knowledge of cancer progression and enhancing the development of more effective treatments.

Therefore, in this study, we apply asymptotic homogenization to model transport processes within a tissue that might represent a tumor mass, with an embedded vascular capillary network, incorporating microscale effects such as vessel geometry and flow patterns into a macroscopic framework. Building upon previous studies [24, 25], we extend the modeling framework by incorporating growth mechanisms as explicit source terms, either through volumetric contributions or mass fluxes driven by chemotactic accretion. By assuming a distinct separation of scales between the typical vessel spacing and the characteristic length of the tissue, we derive differential equations governing the macroscale behavior of the tissue and fluid and nutrient transport. Our methodology involves formulating a system of differential equations through nondimensionalization and scaling, with the asymptotic expansion parameter representing the ratio of vessel distance to the characteristic tissue length scale. The resulting macroscale model for fluid dynamics in the vascular domain is governed by Darcy's law, determining the velocity and pressure fields. In the tumor domain, the dynamics of the ensemble of fluids and cells is described by a modified Darcy's law, where nutrient concentration significantly influences flow. Nutrient transport is modeled across both domains using a coupled advection–diffusion–reaction system, and the interaction between tissue and vascular network is captured through effective mass source terms, reflecting the exchange of nutrients and other essential substances. Effective parameters in the model, which account for the role of microvascular geometry, are computed by solving cell-level differential equations that are coupled with the macroscale governing equations. Although this multiscale coupling poses significant computational challenges, it is possible to obtain computationally manageable systems by assuming additional constraints on the model parameters.

We remark that despite the specific application presented, the developed mathematical method is general and can be applied to the description of other problems in different contexts governed by stationary balance equations and chemical exchange processes, typically modeled by diffusion–advection–reaction problems. Notable examples include the transport of nutrients from tree roots into the soil [32] or a system of aquifers exchanging liquids and chemicals with the surrounding rock domain [33, 34], as well as peatlands [35].

The paper is organized as follows: Section 2 presents the balance equations and their corresponding boundary and interface conditions within the physical domain, distinguishing between the tumor tissue and vessel compartment. Section 3 introduces the governing equations in a non-dimensional form. Section 4 applies a two-scale asymptotic expansion to derive the effective governing equations that describe the physical behavior at the tissue scale. In Section 4.2.1, we explore a particular case that simplifies the computational complexity of the model, making it more tractable for numerical investigation in future work.

Finally, Section 5 offers concluding remarks and future research perspectives.

2 | Balance Equations

We consider a domain $\Omega \subset \mathbb{R}^3$, where $\Omega = \Omega_t \cup \Omega_v$, with Ω_t and Ω_v representing the tumor tissue and the vessel network, respectively. The flow of fluid in both domains, as well as the motion of the ensemble of cells, treated as a fluid, in the tissue region must satisfy mass and momentum balances, which vary in form depending on the specific portion of the domain under consideration. The movement and proliferation of cells are guided by the availability of nutrients. The chemical transport in both regions obeys an advection–diffusion–reaction equation, with different coefficients in each domain. The final problem thus involves determining the unknown fields of interest, namely, the pressure p, the velocity $\boldsymbol{u}$, and the concentration of the nutrients c, which are functions of both space $\boldsymbol{x}$ and time t. The restrictions of these fields to the tissue and vessel compartments are denoted by the subscripts t and v, respectively. We will first analyze the fluid and nutrients transport in each portion of Ω, followed by establishing appropriate interface conditions on $\Gamma = \partial\Omega_t \cap \partial\Omega_v$ to finalize the coupled differential problem. To apply asymptotic homogenization techniques, we further assume that the typical mean distance between fluid vessels, d, is small compared to the characteristic length L of the tissue domain (see Figure 1). This assumption aligns with the biological scenario considered, as the characteristic intercapillary distance is on the order of 50 μm [36], whereas the characteristic size of a vascular tumor can range from a few millimeters to centimeters [37, 38]. Therefore, we define an appropriate spatial scale ratio as follows:

$$\varepsilon = \frac{d}{L} \ll 1. \tag{1}$$

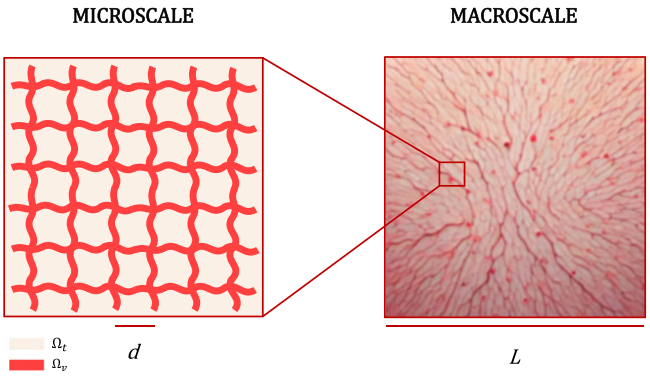

FIGURE 1 | A 2D schematic representation of the microscale and macroscale domains. This illustration highlights the distinction between the microscale dimension d and the typical macroscale dimension L, which defines the homogenized domain where the detailed vessel geometry is averaged and smoothed out. We remark that individual blood vessels are not resolved at the macroscopic scale, and the image is intended for illustrative purposes only. [Colour figure can be viewed at wileyonlinelibrary.com]

2.1 | Tumor Tissue Domain

The tumor region Ω_t is considered as a porous medium composed of a mixture of cells and biological fluid, flowing through a rigid scaffold of extracellular matrix. The extracellular porous scaffold is assumed to be homogeneously distributed in Ω_t and to be neither produced nor degraded by cells. Furthermore, the interstitial fluid and the cells can be collectively treated as a single Newtonian fluid, to which Darcy's law is applicable [39–41]. Thus, inside Ω_t, the biological fluid velocity $\boldsymbol{u}_t$ is related to the gradient of the pressure field p_t through the symmetric and positive-definite second-order tensor K, which is related to permeability of the medium and the viscosity of the fluid phase. Therefore, the following relation holds:

$$\boldsymbol{u}_t = -\mathsf{K}(\boldsymbol{x})\nabla p_t \quad \text{in } \Omega_t. \tag{2}$$

Additionally, the ensemble of cells and biological fluid inside Ω_t should satisfy the mass balance law. Assuming the intrinsic incompressibility of the biological material, which is mostly composed by water, it is possible to take the density of ensemble of cells and liquid constant in time, so that the following equations describe the behavior inside Ω_t

$$\nabla \cdot \boldsymbol{u}_t = \Gamma_t(c_t) + \nabla \cdot \boldsymbol{m}_i(c_t) \quad \text{in } \Omega_t\,. \tag{3}$$

The first term on the r.h.s. of (3) represents volumetric growth, while the second term corresponds to a nonconvective mass flux. Both terms may be influenced by nutrient availability (along with other potential factors), represented, in this work, by a single general nutrient species (e.g., oxygen) with volume concentration $c_t(\boldsymbol{x}, t)$. Nutrients that are provided by the vessel network are transported by $\boldsymbol{u}_t$ and diffused with diffusion coefficient represented by the symmetric, positive-definite, second-order tensors $\mathsf{D}_t(\boldsymbol{x})$ inside Ω_t. The diffusion coefficient is a tensor that can vary in space and can be anisotropic in general, being affected by the local extracellular matrix alignment. Furthermore, nutrients are consumed, with an uptake rate h. Thus, the concentration per unit volume of the generic chemical species obeys the following advection–diffusion–reaction equation

$$\frac{\partial c_t}{\partial t} + \nabla \cdot \left(c_t \boldsymbol{u}_t - \mathsf{D}_t(\boldsymbol{x})\nabla c_t\right) = -h c_t \quad \text{in } \Omega_t\,. \tag{4}$$

We remark that in principle, the uptake rate h and the diffusion coefficient $\mathsf{D}_t(\boldsymbol{x})$ should depend on the tumor cell density. However, consistent with the hypothesis of an inert, rigid, and homogeneously distributed extracellular matrix, this dependency can be disregarded.

In the following, the system of Equations (2–4) is specialized to describe the motion of fluids and nutrients inside a tumor domain. Thus, for the volumetric growth in Equation (3), we will set $\Gamma_t = \gamma c_t$, considering a net proliferation inside the tissue domain proportional to the amount of chemical. However, if the parameter γ is set to zero, the closed mass assumption is retrieved and the growth of the cellular phase occurs at the expense of the biological fluid phase [39]. In the following, for the sake of generality, we allow $\gamma \neq 0$. With slight modification, the present work can also be easily adapt to include another volumetric source, for example representing the role of fluid exchanged between the

interstitium and an additional network of vessels (see, e.g., [42] where the vascularization is considered as a source term rather than geometrically resolved). For instance, the effect of the lymphatic system could be capture by considering a source term of the form $\Gamma_t = \beta_{LS}(p_t - p_{LS})$, being p_{LS} the pressure of the lymphatic system, assumed to be given, and β_{LS} a coefficient related to the permeability of the lymphatic wall and the surface area of lymphatic vessels per unit of tissue volume [43, 44].

Regarding the nonconvective mass flux $\boldsymbol{m}_i$ in Equation (3), it may be related to the chemotactic expansion of cells driven by a nutrient gradient [45, 46]. Following the model proposed in [41, 47], where the flux $\boldsymbol{m}_i$ represents an accretion of mass that enables the chemotactic expansion of the tumor mass, we set the following:

$$\boldsymbol{m}_i = \mathsf{X}(\boldsymbol{x})\nabla c_t, \tag{5}$$

being $\mathsf{X}(\boldsymbol{x})$ the chemotactic tensor. We note that the chemotactic tensor may, in principle, depend on c_t [45, 46]. However, as a first approximation, this dependency can be neglected [46, 48, 49].

Finally, since the motion and diffusion of cells and liquid inside the tissue all follows the orientation of the extracellular matrix fibers, we assume that the tensors representing the diffusion and motion of fluids and cells share the same preferential directions. Thus, defining $\mathsf{A}(\boldsymbol{x})$ the positive-definite preferential direction tensor, encoding information about the microstructural geometry, and guiding the movement of cells and fluids [50–52], we can set $\mathsf{K}(\boldsymbol{x}) = \kappa\mathsf{A}(\boldsymbol{x})$, $\mathsf{X}(\boldsymbol{x}) = \chi(\boldsymbol{x})\mathsf{A}(\boldsymbol{x})$, and $\mathsf{D}_t(\boldsymbol{x}) = D_t\mathsf{A}(\boldsymbol{x})$. In the context of biological tissues, the preferential direction tensor could be derived from diffusion tensor imaging (DTI), which maps the tissue microstructural architecture by determining water diffusion directions [53, 54]. This procedure allows to reconstruct a realistic geometry and environment, with the aim of providing a framework based on patient-specific information. The parameter κ is the hydraulic conductivity, which is related to the tissue permeability k and the dynamic viscosity μ by the following relation:

$$\kappa = \frac{k}{\mu}. \tag{6}$$

Moreover, D_t represents the diffusion coefficient in the tissue, while $\chi(\boldsymbol{x})$ is the chemotactic coefficient. It is worth noting that, unlike the other parameters, $\chi(\boldsymbol{x})$ varies spatially, depending on $\boldsymbol{x}$ within the domain. This is due to retain in the model the fact that cells in different locations may respond differently to chemotaxis. On the other hand, for what concerns the permeability and diffusion, the dependency on space can be kept only inside the preferential direction tensor. Furthermore, we note that while κ and D_t are positive coefficients, the chemotactic coefficient $\chi(\boldsymbol{x})$ may be either positive or negative [45].

2.2 | Vessel Network Domain

Inside the vessel network Ω_v, the motion of the fluid, modeled as an incompressible Newtonian fluid, neglecting inertial effects and body forces, can be appropriately described by the following Stokes flow:

$$\mu\Delta\boldsymbol{u}_v = \nabla p_v \quad \text{in } \Omega_v, \tag{7}$$

$$\nabla \cdot \boldsymbol{u}_v = 0 \quad \text{in } \Omega_v, \tag{8}$$

where μ is a positive parameter representing the dynamic viscosity of the fluid. In the context of this work, the fluid inside the vessel network represents blood, which, generally speaking, is a non-Newtonian fluid composed of plasma and red blood cells [55–57]. However, in vessels much larger than red blood cells, at constant temperature and hematocrit, blood can be assumed, as a first approximation, to behave like a Newtonian fluid, with a viscosity greater than that of plasma [25, 57].

Finally, the nutrients concentration c_v in the capillary network can be described by an advection–diffusion equation as follows:

$$\frac{\partial c_v}{\partial t} + \nabla \cdot \left(c_v\boldsymbol{u}_v - \mathsf{D}_v(\boldsymbol{x})\nabla c_v\right) = 0 \quad \text{in } \Omega_v\,, \tag{9}$$

being $\mathsf{D}_v(\boldsymbol{x})$ the symmetric, positive-definite, second-order tensors representing nutrients diffusion inside the blood. In the following, we will assume $\mathsf{D}_v(\boldsymbol{x}) = D_v\mathsf{A}(\boldsymbol{x})$, considering that diffusion follows the preferential directions dictated by the environment's microstructure, even within the vessel domain. Finally, we observe that nutrient consumption/decay inside the vessel domain is disregarded.

2.3 | Interface Conditions

To close the problem, appropriate conditions should be prescribed at the boundary between the tissue and vessel network domains. In the context of the present paper, we consider a tissue comprising a fluid phase that continuously exchanges with the surrounding vasculature, along with nutrients. By assuming that the Kedem–Katchalsky formulation [58] applies to both the fluid flux J_b and the nutrients flux J_d, we derive the following:

$$J_b = L_p\left[\left(p_v - p_t\right) - \sigma RT\left(c_v - c_t\right)\right], \tag{10}$$

$$J_d = J_b(1-\sigma)c_v + K_d\left(c_v - c_t\right), \tag{11}$$

The parameter L_p stands for the hydraulic permeability of the vessel wall, which governs the fluid leakage from the capillaries. In tumor-induced vessels, this conductivity can be significantly elevated, potentially up to two orders of magnitude higher than in healthy tissue vessels, due to the presence of openings and defects characteristic of tumor vascular networks [59]. Additionally, R denotes the universal gas constant, T represents the absolute temperature, and K_d stands for the diffusive permeability of the vessel wall. The osmotic reflection coefficient $0 \le \sigma \le 1$ measures the membrane's selectivity for the solute and depends on the relative geometry and size of the specific molecule and the membrane pores. For an ideally fully impermeable membrane (which allows no solute flux due to convection), $\sigma = 1$, maximizing osmotic flow. Conversely, for an unselective membrane, $\sigma = 0$, indicating no osmosis and the transport of solutes entirely carried by the fluid flow. Therefore, Equation (11) outlines that the nutrients flux across the vessel membrane comprises a convective component, proportional to the fluid flux, and a diffusive component, proportional to the concentration differential, whereas Equation (10) represents that the flux of fluid across the

vessel interface results from both the hydrostatic pressure gradient and the osmotic pressure disparity, with the latter being directly related to the difference in concentration for dilute solutions. We observe that, in general, the concentration of all chemicals dissolved in blood should be considered in the osmotic pressure disparity [60, 61]. Specifically, in healthy vessels, only the large molecules, such as proteins and in particular albumin, can induce a significant osmotic pressure gradient. Since the concentration of this large molecules can reasonably be taken constant, the oncotic pressure (i.e., the osmotic pressure exerted by plasma proteins, particularly albumin) transmural gradient is generally taken as a constant (equal to 25 mmHg) [60, 61]. On the contrary, in tumor-induced vessels, it is possible to assume that solutes such as oxygen can significantly contribute to the oncotic pressure [25, 59].

It is important to note that Equation (11) represents a linearized form of the relationship established in [25]. This linearization is particularly valid for extreme values of Pe_v, the transvascular Péclet number, which quantifies the relative importance of convection versus diffusion across capillary walls.

In order to impose the correct interface conditions, we assume continuity of the nutrients and fluid fluxes through the interface boundary $\Gamma = \partial\Omega_t \cap \partial\Omega_v$:

$$\boldsymbol{u}_t \cdot \boldsymbol{n} = \boldsymbol{u}_v \cdot \boldsymbol{n} = \tilde{J}_b, \tag{12}$$

$$\left(c_t \boldsymbol{u}_t - D_t \mathsf{A}(\boldsymbol{x})\nabla c_t\right) \cdot \boldsymbol{n} = \left(c_v \boldsymbol{u}_v - D_v \mathsf{A}(\boldsymbol{x})\nabla c_n\right) \cdot \boldsymbol{n} = \tilde{J}_d. \tag{13}$$

Here, $\boldsymbol{n}$ represents the outward unit vector normal to the capillary surface, while we denote by

$$\tilde{J}_b = J_b\left(\hat{p}_v, p_t, c_v, c_t\right), \tag{14}$$

$$\tilde{J}_d = J_d\left(\hat{p}_v, p_t, c_v, c_t\right), \tag{15}$$

the flux prescriptions, given in their general form by (10) and (11), which are functions of the normal component of the viscous stress rather than solely the pressure [25]. Specifically, we adopt the following formulation [26]:

$$\hat{p}_v = p_v - 2\mu\left[\mathsf{E}\left(\boldsymbol{u}_v\right)\boldsymbol{n}\right] \cdot \boldsymbol{n}\,, \tag{16}$$

where $\hat{p}_v$ is the normal component of the stress tensor in the vessels' compartment and $\mathsf{E}(\boldsymbol{u}_v)$ is the symmetric part of the velocity gradient defined as follows:

$$\mathsf{E}(\boldsymbol{u}_v) = \frac{1}{2}\left(\nabla \boldsymbol{u}_v + (\nabla \boldsymbol{u}_v)^T\right)\,. \tag{17}$$

We remark that in many work on physiological blood flux transport and exchange with the tissue [43, 44, 62], the viscous term in (16) is usually neglected. However, boundary conditions involving the Stokes' pressure should include the viscous contribution as well in order to get a coherent variational form of the problem and well-posedness [63], along with convenient a priori estimates for the convergence of the homogenization process [13]. In order to close the problem, an additional boundary condition is required for the tangential components of the fluid velocity in the capillaries. Given that the solid compartment acts as a porous medium, as per, for example, References [13, 24, 26], we assume that the following Beavers–Joseph–Saffman slip conditions [64–66] apply:

$$\boldsymbol{u}_v \cdot \boldsymbol{\tau} = -\frac{\sqrt{k}}{\alpha}\left[2\mathsf{E}(\boldsymbol{u}_v)\boldsymbol{n}\right] \cdot \boldsymbol{\tau}\,. \tag{18}$$

Equation (18) relates the tangent component of the stress to the tangent component of the velocity. In particular, α is a nondimensional parameter that depends on the properties of the porous interface, $\boldsymbol{\tau}$ is any unit vector tangent to the capillary surface, $\mathsf{E}(\boldsymbol{u}_v)$ is the symmetric strain tensor defined in (17), and k is the tissue permeability, which is related to the hydraulic conductivity by relation (6). We further note that since the flow is assumed to be anisotropic, alternative formulations could be considered in place of (18), which would replace the role of the tissue permeability parameter k, for example, involving the trace of the full permeability tensor [20] or the tangential projection of its tangent component [67]. While our model could readily accommodate such alternatives, since there is neither agreement on the specific modification that should be carried out nor consensus on the appropriateness of the interface conditions (18) as such [68], we have chosen to embrace the most standard formulation of such conditions. The latter are however encoding the role of the properties of the interface and reduce to the two crucial limit cases that are most usually explored in practice: the no-slip conditions (for small permeabilities k) and the free-slip conditions (formally for large permeabilities k).

3 | The System of Pdes in Nondimensional Form

Equations (2), (3), (4), (7), (8), and (9), along with the interface conditions (12), (13), and (18), as well as the appropriate flux prescriptions such as (10) and (11), form a coupled system of partial differential equations (PDEs). These equations govern the variables $\boldsymbol{u}_t$, $\boldsymbol{u}_v$, p_t, p_v, c_t, and c_v over the entire domain Ω, which includes both the tumor microenvironment Ω_t and the capillary network Ω_v. For the system to be well-defined, appropriate initial conditions and external boundary conditions on $\partial\Omega$ must be prescribed, tailored to the specific physical system being modeled. We now express the system using nondimensional variables as follows:

$$x = Lx'\,,\quad \boldsymbol{u} = \frac{Cd^2}{\mu}\boldsymbol{u}'\,,\quad p = CLp'\,,\quad c = C_r c'\,,\quad t = \frac{L\mu}{Cd^2}t'\,, \tag{19}$$

where C_r and C are the reference nutrients concentration and pressure gradient, respectively. Additionally, we recall (1), where we have defined the ratio between d and L as ε.

Furthermore, as previously discussed in [25, 26], it is essential to ensure that the total fluid flux (which is proportional to J_b by the total vessel surface area) remains finite as more vessels or channels are added within a fixed portion of the domain, or equivalently, as $\varepsilon \to 0$ (see Equation (1)). This can be managed by noting that the parameters L_p and K_d are typically measured with respect to the total fluid flux. Since the latter is also proportional to the total vessel surface, which scales with the number of vessels (i.e., $\sim 1/\varepsilon$), it is assumed that the specific flux (per unit

surface) scales as $O(\varepsilon)$. We account for this asymptotic behavior of the fluid flux by redefining the parameters accordingly:

$$L_p = \varepsilon L_p^*\,, \quad K_d = \varepsilon K_d^*. \tag{20}$$

The corresponding system of partial differential equations in nondimensional form is then given by the following (with primes omitted for simplicity):

$$\boldsymbol{u}_t = -\overline{\kappa}\overline{\mathsf{A}}(\boldsymbol{x})\nabla p_t \quad \text{in } \Omega_t, \tag{21}$$

$$\nabla\cdot\boldsymbol{u}_t = \overline{\gamma}c_t + \nabla\cdot\left(\overline{\chi}(\boldsymbol{x})\overline{\mathsf{A}}(\boldsymbol{x})\nabla c_t\right) \quad \text{in } \Omega_t\,, \tag{22}$$

$$\varepsilon^2\Delta\boldsymbol{u}_v = \nabla p_v \quad \text{in } \Omega_v, \tag{23}$$

$$\nabla\cdot\boldsymbol{u}_v = 0 \quad \text{in } \Omega_v, \tag{24}$$

$$\frac{\partial c_t}{\partial t} + \nabla\cdot\left(c_t\boldsymbol{u}_t - \overline{D}_t\overline{\mathsf{A}}(\boldsymbol{x})\nabla c_t\right) = -\overline{h}c_t \quad \text{in } \Omega_t, \tag{25}$$

$$\frac{\partial c_v}{\partial t} + \nabla\cdot\left(c_v\boldsymbol{u}_v - \overline{D}_v\overline{\mathsf{A}}(\boldsymbol{x})\nabla c_v\right) = 0 \quad \text{in } \Omega_v, \tag{26}$$

supplemented by the interface conditions:

$$\boldsymbol{u}_v\cdot\boldsymbol{n} = \boldsymbol{u}_t\cdot\boldsymbol{n} = \varepsilon\overline{\mathcal{J}}_b \quad \text{on } \Gamma, \tag{27}$$

$$\boldsymbol{u}_v\cdot\boldsymbol{\tau} = -\varepsilon\overline{\theta}\left[\left(\nabla\boldsymbol{u}_v\right)\boldsymbol{n}\right]\cdot\boldsymbol{\tau} \quad \text{on } \Gamma, \tag{28}$$

$$\left(c_v\boldsymbol{u}_v - \overline{D}_v\overline{\mathsf{A}}(\boldsymbol{x})\nabla c_n\right)\cdot\boldsymbol{n} = \left(c_t\boldsymbol{u}_t - \overline{D}_t\overline{\mathsf{A}}(\boldsymbol{x})\nabla c_t\right)\cdot\boldsymbol{n} = \varepsilon\overline{\mathcal{J}}_d \quad \text{on } \Gamma. \tag{29}$$

Here, $\overline{\mathcal{J}}_b$ and $\overline{\mathcal{J}}_d$ represent the nondimensional fluid and nutrients fluxes, defined as follows:

$$\overline{\mathcal{J}}_b = \overline{L}_p\left(\hat{p}_v - p_t\right) - \overline{\Pi}\left(c_v - c_t\right), \tag{30}$$

$$\overline{\mathcal{J}}_d = \overline{\mathcal{J}}_b(1-\sigma)c_v + \overline{\Upsilon}\left(c_v - c_t\right), \tag{31}$$

where $\hat{p}_v$ is the nondimensional normal stress given by the following:

$$\hat{p}_v = p_v - 2\varepsilon^2\left[\mathsf{E}\left(\boldsymbol{u}_v\right)\boldsymbol{n}\right]\cdot\boldsymbol{n}. \tag{32}$$

The nondimensional numbers, tensors, and functions introduced above are defined as follows:

$$\begin{aligned}
&\overline{\mathsf{A}}(\boldsymbol{x}) = \mathsf{A}(L\boldsymbol{x})\,, \quad \overline{\kappa} = \kappa\frac{\mu}{d^2},\\
&\overline{\gamma} = \gamma\frac{C_rL\mu}{Cd^2}\,, \quad \overline{\chi}(\boldsymbol{x}) = \chi(L\boldsymbol{x})\frac{C_r\mu}{Cd^2L}\,,\\
&\overline{D}_v = D_v\frac{\mu}{Cd^2L}\,, \quad \overline{D}_t = D_t\frac{\mu}{Cd^2L}\,,\\
&\overline{h} = h\frac{L\mu}{Cd^2}\,, \quad \overline{L}_p = L_p^*\frac{\mu L^2}{d^3}\,,\\
&\overline{\Pi} = \frac{\mu LL_p\sigma RTC_r}{Cd^3}\,, \quad \overline{\theta} = \frac{\sqrt{\kappa}}{\alpha}\,, \quad \overline{\Upsilon} = K_d^*\frac{\mu L}{Cd^3}\,.
\end{aligned} \tag{33}$$

4 | Multiscale Formulation

In this section, we use the two-scale technique to derive a continuum macroscale model for the system of Equations (21–29). Given that $\varepsilon \ll 1$, we enforce a sharp separation between the intercapillary distance d (the microscale) and the tissue characteristic dimension L (the macroscale) and define the following:

$$\boldsymbol{y} := \frac{\boldsymbol{x}}{\varepsilon}. \tag{34}$$

In line with standard multiscale analysis [25, 26], $\boldsymbol{x}$ and $\boldsymbol{y}$ are treated as independent variables representing the macrospatial and microspatial scales, respectively. We assume that any unknown field, such as $\boldsymbol{u}_t$, $\boldsymbol{u}_v$, p_t, p_v, c_t and c_v, depends on these independent spatial variables, which transforms the differential operator as follows:

$$\nabla \to \nabla_{\boldsymbol{x}} + \frac{1}{\varepsilon}\nabla_{\boldsymbol{y}}. \tag{35}$$

For each field, we perform a multiple scales expansion in a power series of ε as follows:

$$\boldsymbol{u}(\boldsymbol{x}) = \boldsymbol{u}^\varepsilon(\boldsymbol{x},\boldsymbol{y},t) = \sum_{l=0}^{\infty}\boldsymbol{u}^{(l)}(\boldsymbol{x},\boldsymbol{y},t)\varepsilon^l, \tag{36}$$

$$p(\boldsymbol{x}) = p^\varepsilon(\boldsymbol{x},\boldsymbol{y},t) = \sum_{l=0}^{\infty}p^{(l)}(\boldsymbol{x},\boldsymbol{y},t)\varepsilon^l, \tag{37}$$

$$c(\boldsymbol{x}) = c^\varepsilon(\boldsymbol{x},\boldsymbol{y},t) = \sum_{l=0}^{\infty}c^{(l)}(\boldsymbol{x},\boldsymbol{y},t)\varepsilon^l. \tag{38}$$

We assume periodicity in the microscale variable, so each component is $\boldsymbol{y}$-periodic. As such, all the fields $\boldsymbol{u}^\varepsilon(\boldsymbol{x},\boldsymbol{y},t)$, $p^\varepsilon(\boldsymbol{x},\boldsymbol{y},t)$, and $c^\varepsilon(\boldsymbol{x},\boldsymbol{y},t)$, as well as $\overline{\chi}(\boldsymbol{x},\boldsymbol{y})$ and $\overline{\mathsf{A}}(\boldsymbol{x},\boldsymbol{y})$ are assumed $\boldsymbol{y}$-periodic.

We also assume macroscopic uniformity, meaning that, although we consider a scenario where the geometry can be locally arbitrarily complex and anisotropic, the periodic cell itself does not depend on the macroscale variable $\boldsymbol{x}$. This is a common assumption in asymptotic homogenization, as illustrated for instance in [69], and it is equivalent to assuming that we can identify the microscale domain with a single periodic cell, which is the same for every point of the macroscale domain [70]. Generalization to nonmacroscopic uniformity can be carried out via different approaches (see, e.g., [25] versus [14]). Thus, we assume the following: [26]:

$$\nabla_{\boldsymbol{x}}\cdot\int_\Omega(\bullet)d\boldsymbol{y} = \int_\Omega\nabla_{\boldsymbol{x}}\cdot(\bullet)d\boldsymbol{y}. \tag{39}$$

The aim of this section is to derive a closed system of PDEs for the leading-order variables $\boldsymbol{u}_t^{(0)}$, $\boldsymbol{u}_v^{(0)}$, $p_t^{(0)}$, $p_v^{(0)}$, $c_t^{(0)}$, and $c_v^{(0)}$ over the macroscale domain represented by the variable $\boldsymbol{x}$. This is achieved by exploiting the conditions that arise from equating terms of the same order of ε in Equations (21–29). To focus on obtaining a system of PDEs that applies solely to the macroscale, we introduce the following cell average operator:

$$\langle\bullet\rangle_s = \frac{1}{|\Omega_s|}\int_{\Omega_s}(\bullet)d\boldsymbol{y}\,, \quad s = t,\ v. \tag{40}$$

Exploiting the spatial scale decoupling (35), Equations (21–29) read the following (after multiplying each of them by an appropriate power of ε):

$$\varepsilon \boldsymbol{u}_t = -\varepsilon\overline{\kappa}\overline{\mathsf{A}}(\boldsymbol{x},\boldsymbol{y})\nabla_{\boldsymbol{x}} p_t - \overline{\kappa}\overline{\mathsf{A}}(\boldsymbol{x},\boldsymbol{y})\nabla_{\boldsymbol{y}} p_t \quad \text{in } \Omega_t, \tag{41}$$

$$\begin{aligned}
&\varepsilon^2\nabla_{\boldsymbol{x}}\cdot\boldsymbol{u}_t + \varepsilon\nabla_{\boldsymbol{y}}\cdot\boldsymbol{u}_t \\
&= \varepsilon^2\overline{\gamma}c_t + \varepsilon^2\nabla_{\boldsymbol{x}}\cdot(\overline{\chi}(\boldsymbol{x},\boldsymbol{y})\overline{\mathsf{A}}(\boldsymbol{x},\boldsymbol{y})\nabla_{\boldsymbol{x}}c_t) \\
&\quad + \varepsilon\nabla_{\boldsymbol{x}}\cdot(\overline{\chi}(\boldsymbol{x},\boldsymbol{y})\overline{\mathsf{A}}(\boldsymbol{x},\boldsymbol{y})\nabla_{\boldsymbol{y}}c_t) \\
&\quad + \varepsilon\nabla_{\boldsymbol{y}}\cdot(\overline{\chi}(\boldsymbol{x},\boldsymbol{y})\overline{\mathsf{A}}(\boldsymbol{x},\boldsymbol{y})\nabla_{\boldsymbol{x}}c_t) \\
&\quad + \nabla_{\boldsymbol{y}}\cdot(\overline{\chi}(\boldsymbol{x},\boldsymbol{y})\overline{\mathsf{A}}(\boldsymbol{x},\boldsymbol{y})\nabla_{\boldsymbol{y}}c_t) \quad \text{in } \Omega_t\,,
\end{aligned} \tag{42}$$

$$\begin{aligned}
&\varepsilon^3\Delta_{\boldsymbol{x}}\boldsymbol{u}_v + \varepsilon^2\nabla_{\boldsymbol{x}}\cdot\left(\nabla_{\boldsymbol{y}}\boldsymbol{u}_v\right) + \varepsilon^2\nabla_{\boldsymbol{y}}\cdot\left(\nabla_{\boldsymbol{x}}\boldsymbol{u}_v\right) + \varepsilon\Delta_{\boldsymbol{y}}\boldsymbol{u}_v \\
&= \varepsilon\nabla_{\boldsymbol{x}}p_v + \nabla_{\boldsymbol{y}}p_v \quad \text{in } \Omega_v\,,
\end{aligned} \tag{43}$$

$$\nabla_{\boldsymbol{y}}\cdot\boldsymbol{u}_v + \varepsilon\nabla_{\boldsymbol{x}}\cdot\boldsymbol{u}_v = 0 \quad \text{in } \Omega_v, \tag{44}$$

$$\begin{aligned}
&\varepsilon^2\frac{\partial c_t}{\partial t} + \nabla_{\boldsymbol{x}}\cdot\left(\varepsilon^2 c_t\boldsymbol{u}_t - \varepsilon^2\overline{D}_t\overline{\mathsf{A}}(\boldsymbol{x},\boldsymbol{y})\nabla_{\boldsymbol{x}}c_t - \varepsilon\overline{D}_t\overline{\mathsf{A}}(\boldsymbol{x},\boldsymbol{y})\nabla_{\boldsymbol{y}}c_t\right) \\
&+ \nabla_{\boldsymbol{y}}\cdot\left(\varepsilon c_t\boldsymbol{u}_t - \varepsilon\overline{D}_t\overline{\mathsf{A}}(\boldsymbol{x},\boldsymbol{y})\nabla_{\boldsymbol{x}}c_t - \overline{D}_t\overline{\mathsf{A}}(\boldsymbol{x},\boldsymbol{y})\nabla_{\boldsymbol{y}}c_t\right) \\
&= -\varepsilon^2\overline{h}c_t \quad \text{in } \Omega_t\,,
\end{aligned} \tag{45}$$

$$\begin{aligned}
&\varepsilon^2\frac{\partial c_v}{\partial t} + \nabla_{\boldsymbol{x}}\cdot\left(\varepsilon^2 c_v\boldsymbol{u}_v - \varepsilon^2\overline{D}_v\overline{\mathsf{A}}(\boldsymbol{x},\boldsymbol{y})\nabla_{\boldsymbol{x}}c_v - \varepsilon\overline{D}_v\overline{\mathsf{A}}(\boldsymbol{x},\boldsymbol{y})\nabla_{\boldsymbol{y}}c_v\right) \\
&+ \nabla_{\boldsymbol{y}}\cdot\left(\varepsilon c_v\boldsymbol{u}_v - \varepsilon\overline{D}_v\overline{\mathsf{A}}(\boldsymbol{x},\boldsymbol{y})\nabla_{\boldsymbol{x}}c_v - \overline{D}_v\overline{\mathsf{A}}(\boldsymbol{x},\boldsymbol{y})\nabla_{\boldsymbol{y}}c_v\right) \\
&= 0 \quad \text{in } \Omega_v\,,
\end{aligned} \tag{46}$$

equipped with the following interface conditions:

$$\boldsymbol{u}_v\cdot\boldsymbol{n} = \boldsymbol{u}_t\cdot\boldsymbol{n} = \varepsilon\overline{\mathcal{J}}_b \quad \text{on } \Gamma, \tag{47}$$

$$\boldsymbol{u}_v\cdot\boldsymbol{\tau} = -\varepsilon\overline{\theta}\left[\left(\nabla_{\boldsymbol{x}}\boldsymbol{u}_v\right)\boldsymbol{n}\right]\cdot\boldsymbol{\tau} - \overline{\theta}\left[\left(\nabla_{\boldsymbol{y}}\boldsymbol{u}_v\right)\boldsymbol{n}\right]\cdot\boldsymbol{\tau} \quad \text{on } \Gamma \tag{48}$$

$$\begin{aligned}
&\left(\varepsilon c_v\boldsymbol{u}_v - \varepsilon\overline{D}_v\overline{\mathsf{A}}(\boldsymbol{x},\boldsymbol{y})\nabla_{\boldsymbol{x}}c_v - \overline{D}_v\overline{\mathsf{A}}(\boldsymbol{x},\boldsymbol{y})\nabla_{\boldsymbol{y}}c_v\right)\cdot\boldsymbol{n} \\
&= \left(\varepsilon c_t\boldsymbol{u}_t - \varepsilon\overline{D}_t\overline{\mathsf{A}}(\boldsymbol{x},\boldsymbol{y})\nabla_{\boldsymbol{x}}c_t - \overline{D}_t\overline{\mathsf{A}}(\boldsymbol{x},\boldsymbol{y})\nabla_{\boldsymbol{y}}c_t\right)\cdot\boldsymbol{n} = \varepsilon^2\overline{\mathcal{J}}_d \quad \text{on } \Gamma\,,
\end{aligned} \tag{49}$$

where the general formulation for the fluid nondimensional flux (30) reads as follows:

$$\begin{aligned}
\overline{\mathcal{J}}_b = \overline{L}_p(p_v - p_t) - \overline{\Pi}(c_v - c_t) - \varepsilon^2\left[\frac{1}{2}\left(\nabla_{\boldsymbol{x}}\boldsymbol{u}_v + (\nabla_{\boldsymbol{x}}\boldsymbol{u}_v)^T\right)\boldsymbol{n}\right]\cdot\boldsymbol{n} \\
- \varepsilon\left[\frac{1}{2}\left(\nabla_{\boldsymbol{y}}\boldsymbol{u}_v + (\nabla_{\boldsymbol{y}}\boldsymbol{u}_v)^T\right)\boldsymbol{n}\right]\cdot\boldsymbol{n}\,,
\end{aligned} \tag{50}$$

while nutrients nondimensional flux remains defined by (31).

4.1 | Capillary Fluid Dynamics

We start by considering the capillary problem for fluid and nutrients transport in Ω_v, which is composed by Equations (43), (44), and (46), equipped by interface conditions (47), (48), and (49). Our goal is to establish a closed system for the zero-th order fields $\boldsymbol{u}_v^{(0)}$, $p_v^{(0)}$ and $c_v^{(0)}$. We begin by examining the fluid flow in the capillaries. By collecting terms of order ε^0 in (43), we obtain the following:

$$\nabla_{\boldsymbol{y}}p_v^{(0)} = 0 \Rightarrow p_v^{(0)} = p_v^{(0)}(\boldsymbol{x},t) \quad \text{in } \Omega_v, \tag{51}$$

that means that $p_v^{(0)}$ is $\boldsymbol{y}$-constant. By equating the coefficients of ε^1 in (43) and ε^0 in (44), (47), and (48), we derive the following Stokes-type boundary value problem for $\left(\boldsymbol{u}_v^{(0)}, p_v^{(1)}\right)$:

$$\Delta_{\boldsymbol{y}}\boldsymbol{u}_v^{(0)} = \nabla_{\boldsymbol{x}}p_v^{(0)} + \nabla_{\boldsymbol{y}}p_v^{(1)} \quad \text{in } \Omega_v, \tag{52}$$

$$\nabla_{\boldsymbol{y}}\cdot\boldsymbol{u}_v^{(0)} = 0 \quad \text{in } \Omega_v, \tag{53}$$

$$\boldsymbol{u}_v^{(0)}\cdot\boldsymbol{n} = 0 \quad \text{on } \Gamma, \tag{54}$$

$$\boldsymbol{u}_v^{(0)}\cdot\boldsymbol{\tau} = -\overline{\theta}\left[\left(\nabla_{\boldsymbol{y}}\boldsymbol{u}_v^{(0)}\right)\boldsymbol{n}\right]\cdot\boldsymbol{\tau} \quad \text{on } \Gamma. \tag{55}$$

Next, we utilize the linearity of Equations (52–55), along with (51), to propose the following ansatz for the solution:

$$\boldsymbol{u}_v^{(0)}(\boldsymbol{x},\boldsymbol{y},t) = -\mathsf{W}(\boldsymbol{x},\boldsymbol{y})\nabla_{\boldsymbol{x}}p_v^{(0)}(\boldsymbol{x},t), \tag{56}$$

$$p_v^{(1)}(\boldsymbol{x},\boldsymbol{y},t) = -\boldsymbol{P}_v(\boldsymbol{x},\boldsymbol{y})\cdot\nabla_{\boldsymbol{x}}p_v^{(0)}(\boldsymbol{x},t) + \tilde{p}(\boldsymbol{x},t)\,, \tag{57}$$

where $\tilde{p}(\boldsymbol{x},t)$ represents the part which does not depend on $\boldsymbol{y}$. Moreover, the field $\mathsf{W}(\boldsymbol{x},\boldsymbol{y})$ and the auxiliary vector $\boldsymbol{P}_v(\boldsymbol{x},\boldsymbol{y})$ satisfy the following cell problem:

$$\begin{cases}
\nabla_{\boldsymbol{y}}\boldsymbol{P}_v = \Delta_{\boldsymbol{y}}\mathsf{W}^{\mathrm{T}} + \mathsf{I} & \text{in } \Omega_v\,, \\
\nabla_{\boldsymbol{y}}\cdot\mathsf{W}^{\mathrm{T}} = \boldsymbol{0} & \text{in } \Omega_v\,, \\
\mathsf{W}^{\mathrm{T}}\boldsymbol{n} = \boldsymbol{0} & \text{on } \Gamma\,, \\
-\overline{\theta}\left[\left(\nabla_{\boldsymbol{y}}\mathsf{W}^{\mathrm{T}}\right)\boldsymbol{n}\right]\boldsymbol{\tau} = \mathsf{W}^{\mathrm{T}}\boldsymbol{\tau} & \text{on } \Gamma\,.
\end{cases} \tag{58}$$

The above system of partial differential equations is supplemented by periodicity conditions in $\boldsymbol{y}$ together with suitable conditions that guarantee uniqueness for the auxiliary vector $\boldsymbol{P}_v$, for example,

$$\langle\boldsymbol{P}_v(\boldsymbol{x},\boldsymbol{y})\rangle_v = \boldsymbol{0}. \tag{59}$$

We can now provide a macroscale equation for the average capillary velocity by integrating (56) over Ω_v as follows:

$$\left\langle\boldsymbol{u}_v^{(0)}\right\rangle_v = -\mathsf{M}\nabla_{\boldsymbol{x}}p_v^{(0)}, \tag{60}$$

where $\mathsf{M} = \langle\mathsf{W}\rangle_v$ or componentwise, $M_{ij} = \frac{1}{|\Omega_v|}\int_{\Omega_v} W_{ij}\,d\boldsymbol{y}$. Equation (60) entails that, at the macroscale, the average velocity profile in the capillaries follows an anisotropic form of Darcy's law. The flow is primarily driven by the leading-order

pressure $p_v^{(0)}$ within the capillaries, while the microstructural characteristics are represented by the permeability tensor M.

To derive a macroscale equation for $p_v^{(0)}$, we gather the coefficients of order ε^1 in Equations (44) and (47) as follows:

$$\nabla_{\boldsymbol{y}} \cdot \boldsymbol{u}_v^{(1)} + \nabla_{\boldsymbol{x}} \cdot \boldsymbol{u}_v^{(0)} = 0 \Rightarrow \nabla_{\boldsymbol{x}} \cdot \boldsymbol{u}_v^{(0)} = -\nabla_{\boldsymbol{y}} \cdot \boldsymbol{u}_v^{(1)}, \tag{61}$$

$$\boldsymbol{u}_v^{(1)} \cdot \boldsymbol{n} = \overline{\mathcal{J}}_b^{(0)}. \tag{62}$$

Integrating (61) over Ω_v,

$$\left\langle \nabla_{\boldsymbol{x}} \cdot \boldsymbol{u}_v^{(0)} \right\rangle_v = -\left\langle \nabla_{\boldsymbol{y}} \cdot \boldsymbol{u}_v^{(1)} \right\rangle_v. \tag{63}$$

Exploiting the macroscopic uniformity, the divergence theorem with respect to $\boldsymbol{y}$, and the $\boldsymbol{y}$-periodicity, we obtain the following:

$$\nabla_{\boldsymbol{x}} \cdot \left\langle \boldsymbol{u}_v^{(0)} \right\rangle_v = -\frac{1}{|\Omega_v|} \int_\Gamma \boldsymbol{u}_v^{(1)} \cdot \boldsymbol{n} \, dS_{\boldsymbol{y}}. \tag{64}$$

Using (62), we can write the following:

$$\nabla_{\boldsymbol{x}} \cdot \left\langle \boldsymbol{u}_v^{(0)} \right\rangle_v = -\frac{1}{|\Omega_v|} \int_\Gamma \overline{\mathcal{J}}_b^{(0)} \, dS_{\boldsymbol{y}}. \tag{65}$$

Finally, we can incorporate Equation (60) to derive the equation for the leading-order pressure $p_v^{(0)}$ as follows:

$$\nabla_{\boldsymbol{x}} \cdot \left(\mathsf{M} \nabla_{\boldsymbol{x}} p_v^{(0)} \right) = \frac{1}{|\Omega_v|} \int_\Gamma \overline{\mathcal{J}}_b^{(0)} \, dS_{\boldsymbol{y}}. \tag{66}$$

The fluid flow within the capillaries compartment is not incompressible at the macroscale. The source term on the right-hand side of above equation arises from the leading-order fluid flux $\overline{\mathcal{J}}_b^{(0)}$, defined as follows:

$$\overline{\mathcal{J}}_b^{(0)} = \overline{L}_p (p_v^{(0)} - p_t^{(0)}) - \overline{\Pi}(c_v^{(0)} - c_t^{(0)}). \tag{67}$$

Consequently, the microscale exchange between the tumor and capillary compartments across the interface Γ translates into a volumetric contribution on the global scale.

Finally, a macroscale equation for the leading-order nutrient concentration in the capillaries is derived by collecting the coefficients of ε^0 in (46) and (49) as follows:

$$\nabla_{\boldsymbol{y}} \cdot \left(\overline{D}_v \overline{\mathsf{A}}(\boldsymbol{x}, \boldsymbol{y}) \nabla_{\boldsymbol{y}} c^{(0)} \right) = 0 \quad \text{in } \Omega_v, \tag{68}$$

$$\left(\overline{D}_v \overline{\mathsf{A}}(\boldsymbol{x}, \boldsymbol{y}) \nabla_{\boldsymbol{y}} c^{(0)} \right) \cdot \boldsymbol{n} = 0 \quad \text{on } \Gamma. \tag{69}$$

Equation (68), together with (69) and $\boldsymbol{y}$-periodicity, has a constant solution with respect to $\boldsymbol{y}$, that is,

$$c_v^{(0)} = c_v^{(0)}(\boldsymbol{x}, t), \tag{70}$$

Then, we collect the coefficients of ε^1-terms, obtaining the following:

$$\begin{aligned} &-\nabla_{\boldsymbol{x}} \cdot \left(\overline{D}_v \overline{\mathsf{A}}(\boldsymbol{x}, \boldsymbol{y}) \nabla_{\boldsymbol{y}} c_v^{(0)} \right) \\ &+ \nabla_{\boldsymbol{y}} \cdot \left(c_v^{(0)} \boldsymbol{u}_v^{(0)} - \overline{D}_v \overline{\mathsf{A}}(\boldsymbol{x}, \boldsymbol{y}) \nabla_{\boldsymbol{x}} c_v^{(0)} - \overline{D}_v \overline{\mathsf{A}}(\boldsymbol{x}, \boldsymbol{y}) \nabla_{\boldsymbol{y}} c_v^{(1)} \right) = 0 \quad \text{in } \Omega_v, \end{aligned} \tag{71}$$

$$\left(c_v^{(0)} \boldsymbol{u}_v^{(0)} - \overline{D}_v \overline{\mathsf{A}}(\boldsymbol{x}, \boldsymbol{y}) \nabla_{\boldsymbol{x}} c_v^{(0)} - \overline{D}_v \overline{\mathsf{A}}(\boldsymbol{x}, \boldsymbol{y}) \nabla_{\boldsymbol{y}} c_v^{(1)} \right) \cdot \boldsymbol{n} = 0 \quad \text{on } \Gamma. \tag{72}$$

Then, in Equation (71), we utilize the fact that $c_v^{(0)}$ is $\boldsymbol{y}$-independent and apply (53), while in Equation (72), we apply (54) to derive the following:

$$\nabla_{\boldsymbol{y}} \cdot \left(\overline{\mathsf{A}}(\boldsymbol{x}, \boldsymbol{y}) \nabla_{\boldsymbol{x}} c_v^{(0)} + \overline{\mathsf{A}}(\boldsymbol{x}, \boldsymbol{y}) \nabla_{\boldsymbol{y}} c_v^{(1)} \right) = 0 \quad \text{in } \Omega_v, \tag{73}$$

$$\left(\overline{\mathsf{A}}(\boldsymbol{x}, \boldsymbol{y}) \nabla_{\boldsymbol{x}} c_v^{(0)} + \overline{\mathsf{A}}(\boldsymbol{x}, \boldsymbol{y}) \nabla_{\boldsymbol{y}} c_v^{(1)} \right) \cdot \boldsymbol{n} = 0 \quad \text{on } \Gamma. \tag{74}$$

At this point, we can state the following ansatz:

$$c_v^{(1)}(\boldsymbol{x}, \boldsymbol{y}, t) = -\boldsymbol{a}(\boldsymbol{x}, \boldsymbol{y}) \cdot \nabla_{\boldsymbol{x}} c_v^{(0)}(\boldsymbol{x}, t) + \tilde{c}_v(\boldsymbol{x}, t), \tag{75}$$

where $\tilde{c}_v(\boldsymbol{x}, t)$ represents the part which does not depend on $\boldsymbol{y}$ and the auxiliary vector $\boldsymbol{a}(\boldsymbol{x}, \boldsymbol{y})$ solve the cell problem:

$$\begin{cases} \nabla_{\boldsymbol{y}} \cdot \left[(\nabla_{\boldsymbol{y}} \boldsymbol{a}) \mathsf{A}^{\mathrm{T}} \right] = \nabla_{\boldsymbol{y}} \cdot \mathsf{A}^{\mathrm{T}} & \text{in } \Omega_v, \\ (\nabla_{\boldsymbol{y}} \boldsymbol{a}) \mathsf{A}^{\mathrm{T}} \boldsymbol{n} = \mathsf{A}^{\mathrm{T}} \boldsymbol{n} & \text{on } \Gamma. \end{cases} \tag{76}$$

A further condition for $\boldsymbol{a}$ is required to ensure uniqueness, for example:

$$\langle \boldsymbol{a}(\boldsymbol{x}, \boldsymbol{y}) \rangle_v = \boldsymbol{0}. \tag{77}$$

Next, we aim to derive a macroscale equation for the leading-order concentration in the capillaries $c_v^{(0)}$. We begin by equating the ε^2 coefficients in Equations (46) and (49), resulting in the following:

$$\begin{aligned} &\frac{\partial c_v^{(0)}}{\partial t} + \nabla_{\boldsymbol{x}} \cdot \left(c_v^{(0)} \boldsymbol{u}_v^{(0)} - \overline{D}_v \overline{\mathsf{A}} \nabla_{\boldsymbol{x}} c_v^{(0)} - \overline{D}_v \overline{\mathsf{A}} \nabla_{\boldsymbol{y}} c_v^{(1)} \right) \\ &+ \nabla_{\boldsymbol{y}} \cdot \left(c_v^{(0)} \boldsymbol{u}_v^{(1)} + c_v^{(1)} \boldsymbol{u}_v^{(0)} - \overline{D}_v \overline{\mathsf{A}} \nabla_{\boldsymbol{x}} c_v^{(1)} - \overline{D}_v \overline{\mathsf{A}} \nabla_{\boldsymbol{y}} c_v^{(2)} \right) \\ &= 0 \quad \text{in } \Omega_v, \end{aligned} \tag{78}$$

$$\left(c_v^{(0)} \boldsymbol{u}_v^{(1)} + c_v^{(1)} \boldsymbol{u}_v^{(0)} - \overline{D}_v \overline{\mathsf{A}} \nabla_{\boldsymbol{x}} c_v^{(1)} - \overline{D}_v \overline{\mathsf{A}} \nabla_{\boldsymbol{y}} c_v^{(2)} \right) \cdot \boldsymbol{n} = \overline{\mathcal{J}}_d^{(0)} \quad \text{on } \Gamma, \tag{79}$$

where the zero-th order nutrients flux is given by the following:

$$\overline{\mathcal{J}}_d^{(0)} = \overline{\mathcal{J}}_b^{(0)} (1 - \sigma) c_v^{(0)} + \overline{\Upsilon} \left(c_v^{(0)} - c_t^{(0)} \right) \tag{80}$$

Taking the integral average over Ω_v of the first equation, exploiting the divergence theorem, the $\boldsymbol{y}$-periodicity, and the interface condition given from the second equation, we obtain the following:

$$\begin{aligned} &\frac{\partial c_v^{(0)}}{\partial t} + \nabla_{\boldsymbol{x}} \cdot \left(c_v^{(0)} \left\langle \boldsymbol{u}_v^{(0)} \right\rangle_v \right) - \nabla_{\boldsymbol{x}} \cdot \left(\overline{D}_v \left\langle \overline{\mathsf{A}} \right\rangle_v \nabla_{\boldsymbol{x}} c_v^{(0)} \right) \\ &- \nabla_{\boldsymbol{x}} \cdot \left(\overline{D}_v \left\langle \overline{\mathsf{A}} \nabla_{\boldsymbol{y}} c_v^{(1)} \right\rangle_v \right) + \frac{1}{|\Omega_v|} \int_\Gamma \overline{\mathcal{J}}_d^{(0)} \, dS_{\boldsymbol{y}} = 0 \quad \text{in } \Omega_v. \end{aligned} \tag{81}$$

Using the ansatz, we can write the following:

$$\frac{\partial c_v^{(0)}}{\partial t} + \nabla_{\boldsymbol{x}} \cdot \left(c_v^{(0)} \left\langle \boldsymbol{u}_v^{(0)} \right\rangle_v\right) - \nabla_{\boldsymbol{x}} \cdot \left(\overline{D}_v \left\langle \overline{\mathsf{A}} \right\rangle_v \nabla_{\boldsymbol{x}} c_v^{(0)}\right) + \nabla_{\boldsymbol{x}} \cdot \left(\overline{D}_v \left\langle \overline{\mathsf{A}} (\nabla_{\boldsymbol{y}} \boldsymbol{a})^{\mathrm{T}} \right\rangle_v \nabla_{\boldsymbol{x}} c_v^{(0)}\right) = -\frac{1}{|\Omega_v|} \int_\Gamma \overline{\mathcal{J}}_d^{(0)} \, dS_{\boldsymbol{y}} \quad \text{in } \Omega_v \,. \tag{82}$$

By defining the second-order tensor $\mathsf{D}_v = \overline{D}_v \left\langle \overline{\mathsf{A}} - \overline{\mathsf{A}} (\nabla_{\boldsymbol{y}} \boldsymbol{a})^{\mathrm{T}} \right\rangle_v$, which represents the effective diffusivity tensor for the capillary compartment, we can reformulate Equation (82) to finally obtain the following reaction–diffusion–advection equation for nutrients concentration $c_v^{(0)}$:

$$\frac{\partial c_v^{(0)}}{\partial t} + \nabla_{\boldsymbol{x}} \cdot \left(c_v^{(0)} \left\langle \boldsymbol{u}_v^{(0)} \right\rangle_v - \mathsf{D}_v \nabla_{\boldsymbol{x}} c_v^{(0)}\right) = -\frac{1}{|\Omega_v|} \int_\Gamma \overline{\mathcal{J}}_d^{(0)} \, dS_{\boldsymbol{y}} \quad \text{in } \Omega_v \,. \tag{83}$$

To conclude, the differential problem in the capillary domain is given by (60), (66), and (83) for variables $\left\langle \boldsymbol{u}_v^{(0)} \right\rangle_v$, $p_v^{(0)}$, and $c_v^{(0)}$. The system is not closed, because the fluid and nutrients fluxes $\overline{\mathcal{J}}_b^{(0)}$ and $\overline{\mathcal{J}}_d^{(0)}$ depend on the tumor micro-environment variables too. Hence, we proceed to derive the macroscale differential system for the tumor micro-environment compartment, allowing us to formulate a closed coupled problem involving both capillary and tumor micro-environment variables.

4.2 | Tumor Microenvironment Problem

We consider now the tumor micro-environment problem, which consists of Equations (41), (42), and (45) and the first part of the interface boundary conditions (47) and (49). We start equating coefficients of ε^0 in (41) to obtain the following:

$$-\overline{\kappa}\overline{\mathsf{A}}(\boldsymbol{x}, \boldsymbol{y}) \nabla_{\boldsymbol{y}} p_t^{(0)} = 0 \Rightarrow p_t^{(0)} = p_t^{(0)}(\boldsymbol{x}, t) \quad \text{in } \Omega_t, \tag{84}$$

that means that $p_t^{(0)}$ is $\boldsymbol{y}$-constant.

By equating the coefficients of ε^1 in (41) and (42) and of ε^0 in (47), we obtain the following:

$$\boldsymbol{u}_t^{(0)} = -\overline{\kappa}\overline{\mathsf{A}}(\boldsymbol{x}, \boldsymbol{y}) \nabla_{\boldsymbol{x}} p_t^{(0)} - \overline{\kappa}\overline{\mathsf{A}}(\boldsymbol{x}, \boldsymbol{y}) \nabla_{\boldsymbol{y}} p_t^{(1)} \quad \text{in } \Omega_t, \tag{85}$$

$$\nabla_{\boldsymbol{y}} \cdot \boldsymbol{u}_t^{(0)} = \nabla_{\boldsymbol{x}} \cdot (\overline{\chi}(\boldsymbol{x}, \boldsymbol{y}) \overline{\mathsf{A}}(\boldsymbol{x}, \boldsymbol{y}) \nabla_{\boldsymbol{y}} c_t^{(0)}) + \nabla_{\boldsymbol{y}} \cdot (\overline{\chi}(\boldsymbol{x}, \boldsymbol{y}) \overline{\mathsf{A}}(\boldsymbol{x}, \boldsymbol{y}) \nabla_{\boldsymbol{x}} c_t^{(0)}) + \nabla_{\boldsymbol{y}} \cdot (\overline{\chi}(\boldsymbol{x}, \boldsymbol{y}) \overline{\mathsf{A}}(\boldsymbol{x}, \boldsymbol{y}) \nabla_{\boldsymbol{y}} c_t^{(1)}) \quad \text{in } \Omega_t \,, \tag{86}$$

$$\boldsymbol{u}_t^{(0)} \cdot \boldsymbol{n}_t = 0 \quad \text{on } \Gamma, \tag{87}$$

where $\boldsymbol{n}_t = -\boldsymbol{n}$ is the outward unit vector normal to the tumor micro-environment surface. Now, we can substitute Equation (85) into Equations (86) and (87) to obtain the following:

$$\begin{aligned} &-\nabla_{\boldsymbol{y}} \cdot \left(\overline{\kappa}\overline{\mathsf{A}}(\boldsymbol{x}, \boldsymbol{y}) \nabla_{\boldsymbol{x}} p_t^{(0)} + \overline{\kappa}\overline{\mathsf{A}}(\boldsymbol{x}, \boldsymbol{y}) \nabla_{\boldsymbol{y}} p_t^{(1)}\right) \\ &= \nabla_{\boldsymbol{x}} \cdot (\overline{\chi}(\boldsymbol{x}, \boldsymbol{y}) \overline{\mathsf{A}}(\boldsymbol{x}, \boldsymbol{y}) \nabla_{\boldsymbol{y}} c_t^{(0)}) \\ &\quad + \nabla_{\boldsymbol{y}} \cdot (\overline{\chi}(\boldsymbol{x}, \boldsymbol{y}) \overline{\mathsf{A}}(\boldsymbol{x}, \boldsymbol{y}) \nabla_{\boldsymbol{x}} c_t^{(0)}) \\ &\quad + \nabla_{\boldsymbol{y}} \cdot (\overline{\chi}(\boldsymbol{x}, \boldsymbol{y}) \overline{\mathsf{A}}(\boldsymbol{x}, \boldsymbol{y}) \nabla_{\boldsymbol{y}} c_t^{(1)}) \quad \text{in } \Omega_t \,, \end{aligned} \tag{88}$$

$$\overline{\mathsf{A}}(\boldsymbol{x}, \boldsymbol{y}) \nabla_{\boldsymbol{y}} p_t^{(1)} \cdot \boldsymbol{n}_t = -\overline{\mathsf{A}}(\boldsymbol{x}, \boldsymbol{y}) \nabla_{\boldsymbol{x}} p_t^{(0)} \cdot \boldsymbol{n}_t \quad \text{on } \Gamma. \tag{89}$$

At this stage, we need to derive an equation for the leading-order pressure, $p_t^{(0)}$. Before proceeding with this, we will first derive an equation for the leading-order nutrient concentration, $c_t^{(0)}$, and propose an ansatz for $c_t^{(1)}$, as these quantities are present in Equation (88). To achieve this, we collect the coefficients of ε^0 from Equations (45) and (49) as follows:

$$-\nabla_{\boldsymbol{y}} \left(\overline{D}_t \overline{\mathsf{A}}(\boldsymbol{x}, \boldsymbol{y}) \nabla_{\boldsymbol{y}} c_t^{(0)}\right) = 0 \quad \text{in } \Omega_t, \tag{90}$$

$$\left(\overline{D}_t \overline{\mathsf{A}}(\boldsymbol{x}, \boldsymbol{y}) \nabla_{\boldsymbol{y}} c_t^{(0)}\right) \cdot \boldsymbol{n}_t = 0 \quad \text{on } \Gamma. \tag{91}$$

The first equation, together with periodicity conditions in $\boldsymbol{y}$ and homogeneous Neumann conditions on Γ, has a constant solution with respect to $\boldsymbol{y}$, that is,

$$c_t^{(0)} = c_t^{(0)}(\boldsymbol{x}, t). \tag{92}$$

Collecting terms of order ε^1 in Equations (45) and (49), we obtain the following differential problem:

$$-\nabla_{\boldsymbol{x}} \cdot \left(\overline{D}_t \overline{\mathsf{A}}(\boldsymbol{x}, \boldsymbol{y}) \nabla_{\boldsymbol{y}} c_t^{(0)}\right) + \nabla_{\boldsymbol{y}} \cdot \left(c_t^{(0)} \boldsymbol{u}_t^{(0)} - \overline{D}_t \overline{\mathsf{A}}(\boldsymbol{x}, \boldsymbol{y}) \nabla_{\boldsymbol{x}} c_t^{(0)} - \overline{D}_t \overline{\mathsf{A}}(\boldsymbol{x}, \boldsymbol{y}) \nabla_{\boldsymbol{y}} c_t^{(1)}\right) = 0 \quad \text{in } \Omega_t \,, \tag{93}$$

$$\left(c_t^{(0)} \boldsymbol{u}_t^{(0)} - \overline{D}_t \overline{\mathsf{A}}(\boldsymbol{x}, \boldsymbol{y}) \nabla_{\boldsymbol{x}} c_t^{(0)} - \overline{D}_t \overline{\mathsf{A}}(\boldsymbol{x}, \boldsymbol{y}) \nabla_{\boldsymbol{y}} c_t^{(1)}\right) \cdot \boldsymbol{n}_t = 0 \quad \text{on } \Gamma. \tag{94}$$

Then, in Equation (93), we utilize the fact that $c_t^{(0)}$ is $\boldsymbol{y}$-independent and substitute $\nabla_{\boldsymbol{y}} \cdot \boldsymbol{u}_t^{(0)}$ recalling Equation (86), while in Equation (94), we apply (87) to derive the following:

$$\begin{aligned} &\nabla_{\boldsymbol{y}} \cdot \left[\left(\overline{\chi}(\boldsymbol{x}, \boldsymbol{y}) c_t^{(0)} - \overline{D}_t\right) \overline{\mathsf{A}}(\boldsymbol{x}, \boldsymbol{y}) \nabla_{\boldsymbol{y}} c_t^{(1)}\right] \\ &= -\nabla_{\boldsymbol{y}} \cdot \left[\left(\overline{\chi}(\boldsymbol{x}, \boldsymbol{y}) c_t^{(0)} - \overline{D}_t\right) \overline{\mathsf{A}}(\boldsymbol{x}, \boldsymbol{y}) \nabla_{\boldsymbol{x}} c_t^{(0)}\right] \quad \text{in } \Omega_t \,, \end{aligned} \tag{95}$$

$$\overline{\mathsf{A}}(\boldsymbol{x}, \boldsymbol{y}) \nabla_{\boldsymbol{y}} c_t^{(1)} \cdot \boldsymbol{n}_t = -\overline{\mathsf{A}}(\boldsymbol{x}, \boldsymbol{y}) \nabla_{\boldsymbol{x}} c_t^{(0)} \cdot \boldsymbol{n}_t \quad \text{on } \Gamma. \tag{96}$$

We can then state the following ansatz for $c_t^{(1)}$:

$$c_t^{(1)}(\boldsymbol{x}, \boldsymbol{y}, t) = -\boldsymbol{b}(\boldsymbol{x}, \boldsymbol{y}) \cdot \nabla_{\boldsymbol{x}} c_t^{(0)}(\boldsymbol{x}, t) + \tilde{c}_t(\boldsymbol{x}, t), \tag{97}$$

where $\tilde{c}_t(\boldsymbol{x}, t)$ denotes the component that is independent of $\boldsymbol{y}$ and the auxiliary vector $\boldsymbol{b}(\boldsymbol{x}, \boldsymbol{y})$ solve the following cell problem:

$$\begin{cases} \nabla_{\boldsymbol{y}} \cdot \left[\left(\overline{\chi} c_t^{(0)} - \overline{D}_t\right) (\nabla_{\boldsymbol{y}} \boldsymbol{b}) \overline{\mathsf{A}}^{\mathrm{T}}\right] = \nabla_{\boldsymbol{y}} \cdot \left[\left(\overline{\chi} c_t^{(0)} - \overline{D}_t\right) \overline{\mathsf{A}}^{\mathrm{T}}\right] & \text{in } \Omega_t \,, \\ (\nabla_{\boldsymbol{y}} \boldsymbol{b}) \overline{\mathsf{A}}^{\mathrm{T}} \boldsymbol{n} = \overline{\mathsf{A}}^{\mathrm{T}} \boldsymbol{n} & \text{on } \Gamma \,. \end{cases} \tag{98}$$

A further condition for $\boldsymbol{b}$ is required to ensure uniqueness, for example,

$$\langle \boldsymbol{b}(\boldsymbol{x},\boldsymbol{y})\rangle_t = \boldsymbol{0}. \tag{99}$$

Next, our goal is to derive a macroscale equation for the leading-order concentration $c_t^{(0)}$ in Ω_t. To do this, we start by matching the ε^2 terms in Equations (45) and (49), leading to the following:

$$\begin{aligned}&\frac{\partial c_t^{(0)}}{\partial t} + \nabla_{\boldsymbol{x}}\cdot\left(c_t^{(0)}\boldsymbol{u}_t^{(0)} - \overline{D}_t\overline{\mathsf{A}}\nabla_{\boldsymbol{x}}c_t^{(0)} - \overline{D}_t\overline{\mathsf{A}}\nabla_{\boldsymbol{y}}c_t^{(1)}\right)\\ &+\nabla_{\boldsymbol{y}}\cdot\left(c_t^{(0)}\boldsymbol{u}_t^{(1)} + c_t^{(1)}\boldsymbol{u}_t^{(0)} - \overline{D}_t\overline{\mathsf{A}}\nabla_{\boldsymbol{x}}c_t^{(1)} - \overline{D}_t\overline{\mathsf{A}}\nabla_{\boldsymbol{y}}c_t^{(2)}\right)\\ &= -\overline{h}c_t^{(0)} \quad \text{in } \Omega_t\,,\end{aligned} \tag{100}$$

$$\left(c_t^{(0)}\boldsymbol{u}_t^{(1)} + c_t^{(1)}\boldsymbol{u}_t^{(0)} - \overline{D}_t\overline{\mathsf{A}}\nabla_{\boldsymbol{x}}c_t^{(1)} - \overline{D}_t\overline{\mathsf{A}}\nabla_{\boldsymbol{y}}c_t^{(2)}\right)\cdot\boldsymbol{n}_t = -\overline{\mathcal{J}}_d^{(0)} \quad \text{on } \Gamma, \tag{101}$$

where the zero-th order fluxes $\overline{\mathcal{J}}_b^{(0)}$ and $\overline{\mathcal{J}}_d^{(0)}$ are defined by (67) and (80). Taking the integral average over Ω_t of the first equation, exploiting the divergence theorem, the $\boldsymbol{y}$-periodicity, and the interface condition given from Equation (101), we can rewrite Equation (100) as follows:

$$\begin{aligned}&\frac{\partial c_t^{(0)}}{\partial t} + \nabla_{\boldsymbol{x}}\cdot\left(c_t^{(0)}\left\langle\boldsymbol{u}_t^{(0)}\right\rangle_t\right) - \nabla_{\boldsymbol{x}}\cdot\left(\overline{D}_t\left\langle\overline{\mathsf{A}}\right\rangle_t\nabla_{\boldsymbol{x}}c_t^{(0)}\right)\\ &-\nabla_{\boldsymbol{x}}\cdot\left(\overline{D}_t\left\langle\overline{\mathsf{A}}\nabla_{\boldsymbol{y}}c_t^{(1)}\right\rangle_t\right) - \frac{1}{|\Omega_t|}\int_\Gamma\overline{\mathcal{J}}_d^{(0)}\,dS_{\boldsymbol{y}} = -\overline{h}c_t^{(0)} \quad \text{in } \Omega_t\,.\end{aligned} \tag{102}$$

Using ansatz (97), we can write the following:

$$\begin{aligned}&\frac{\partial c_t^{(0)}}{\partial t} + \nabla_{\boldsymbol{x}}\cdot\left(c_t^{(0)}\left\langle\boldsymbol{u}_t^{(0)}\right\rangle_t\right) - \nabla_{\boldsymbol{x}}\cdot\left(\overline{D}_t\left\langle\overline{\mathsf{A}}\right\rangle_t\nabla_{\boldsymbol{x}}c_t^{(0)}\right)\\ &+\nabla_{\boldsymbol{x}}\cdot\left(\overline{D}_t\left\langle\overline{\mathsf{A}}\left(\nabla_{\boldsymbol{y}}\boldsymbol{b}\right)^{\mathrm{T}}\right\rangle_t\nabla_{\boldsymbol{x}}c_v^{(0)}\right)\\ &= \frac{1}{|\Omega_t|}\int_\Gamma\overline{\mathcal{J}}_d^{(0)}\,dS_{\boldsymbol{y}} - \overline{h}c_t^{(0)} \quad \text{in } \Omega_t\,.\end{aligned} \tag{103}$$

Firstly, we observe that the zero-th order nutrient flux, $\overline{\mathcal{J}}_d^{(0)}$, which appears in the surface integral term on the right-hand side and defined by (80), is independent of $\boldsymbol{y}$ due to the conditions given in (51), (70), (84), and (92). Next, we define the second-order tensor $\mathsf{D}_t = \overline{D}_t\left\langle\overline{\mathsf{A}} - \overline{\mathsf{A}}\left(\nabla_{\boldsymbol{y}}\boldsymbol{b}\right)^{\mathrm{T}}\right\rangle_t$, which represents the effective diffusivity tensor for the tumor compartment. Incorporating these two observations into Equation (103), we obtain the following reaction–diffusion–advection equation for the nutrient concentration $c_t^{(0)}$:

$$\frac{\partial c_t^{(0)}}{\partial t} + \nabla_{\boldsymbol{x}}\cdot\left(c_t^{(0)}\left\langle\boldsymbol{u}_t^{(0)}\right\rangle_t - \mathsf{D}_t\nabla_{\boldsymbol{x}}c_t^{(0)}\right) = \frac{|\Gamma|}{|\Omega_t|}\overline{\mathcal{J}}_d^{(0)} - \overline{h}c_t^{(0)} \quad \text{in } \Omega_t, \tag{104}$$

where $|\Gamma|$ is the total surface of the interface Γ.

We have now to write an equation for the leading order velocity $\boldsymbol{u}_t^{(0)}$ and pressure $p_t^{(0)}$. Examining Equations (88) and (89), we can now rewrite them by considering that $c_t^{(0)}$ is $\boldsymbol{y}$-independent. Furthermore, we can consider the ansatz (97) made for $c_t^{(1)}$:

$$\begin{aligned}&\nabla_{\boldsymbol{y}}\cdot\left(\overline{\kappa}\overline{\mathsf{A}}(\boldsymbol{x},\boldsymbol{y})\nabla_{\boldsymbol{y}}p_t^{(1)}\right) = -\nabla_{\boldsymbol{y}}\cdot\left(\overline{\kappa}\overline{\mathsf{A}}(\boldsymbol{x},\boldsymbol{y})\nabla_{\boldsymbol{x}}p_t^{(0)}\right) +\\ &-\nabla_{\boldsymbol{y}}\cdot\left(\overline{\chi}(\boldsymbol{x},\boldsymbol{y})\overline{\mathsf{A}}(\boldsymbol{x},\boldsymbol{y})\nabla_{\boldsymbol{x}}c_t^{(0)}\right)\\ &+\nabla_{\boldsymbol{y}}\cdot\left(\overline{\chi}(\boldsymbol{x},\boldsymbol{y})\overline{\mathsf{A}}(\boldsymbol{x},\boldsymbol{y})\left(\nabla_{\boldsymbol{y}}\boldsymbol{b}\right)^{\mathrm{T}}\nabla_{\boldsymbol{x}}c_t^{(0)}\right) \text{ in } \Omega_t\,,\end{aligned} \tag{105}$$

$$\overline{\mathsf{A}}(\boldsymbol{x},\boldsymbol{y})\nabla_{\boldsymbol{y}}p_t^{(1)}\cdot\boldsymbol{n}_t = -\overline{\mathsf{A}}(\boldsymbol{x},\boldsymbol{y})\nabla_{\boldsymbol{x}}p_t^{(0)}\cdot\boldsymbol{n}_t \quad \text{on } \Gamma. \tag{106}$$

At this point, we can state the following ansatz:

$$\begin{aligned}p_t^{(1)}(\boldsymbol{x},\boldsymbol{y},t) = &-\boldsymbol{P}_t(\boldsymbol{x},\boldsymbol{y})\cdot\nabla_{\boldsymbol{x}}p_t^{(0)}(\boldsymbol{x},t)\\ &-\boldsymbol{C}_t(\boldsymbol{x},\boldsymbol{y})\cdot\nabla_{\boldsymbol{x}}c_t^{(0)}(\boldsymbol{x},t) + \tilde{p}_t(\boldsymbol{x},t)\,,\end{aligned} \tag{107}$$

where $\tilde{p}_t(\boldsymbol{x},t)$ represents the term independent of $\boldsymbol{y}$ and the auxiliary vector $\boldsymbol{P}_t(\boldsymbol{x},\boldsymbol{y})$ solve the following cell problem:

$$\begin{cases}\nabla_{\boldsymbol{y}}\cdot\left[\left(\nabla_{\boldsymbol{y}}\boldsymbol{P}_t\right)\overline{\mathsf{A}}^{\mathrm{T}}\right] = \nabla_{\boldsymbol{y}}\cdot\overline{\mathsf{A}}^{\mathrm{T}} & \text{in } \Omega_t\,,\\ \left(\nabla_{\boldsymbol{y}}\boldsymbol{P}_t\right)\overline{\mathsf{A}}^{\mathrm{T}}\boldsymbol{n} = \overline{\mathsf{A}}^{\mathrm{T}}\boldsymbol{n} & \text{on } \Gamma\,,\end{cases} \tag{108}$$

while the auxiliary vector $\boldsymbol{C}_t(\boldsymbol{x},\boldsymbol{y})$ solve the cell problem as follows:

$$\begin{cases}\nabla_{\boldsymbol{y}}\cdot\left[\overline{\kappa}\left(\nabla_{\boldsymbol{y}}\boldsymbol{C}_t\right)\overline{\mathsf{A}}^{\mathrm{T}}\right] = \nabla_{\boldsymbol{y}}\cdot\left[\overline{\chi}\overline{\mathsf{A}}^{\mathrm{T}} - \overline{\chi}\left(\nabla_{\boldsymbol{y}}\boldsymbol{b}\right)\overline{\mathsf{A}}^{\mathrm{T}}\right] & \text{in } \Omega_t\,,\\ \left(\nabla_{\boldsymbol{y}}\boldsymbol{C}_t\right)\overline{\mathsf{A}}^{\mathrm{T}}\boldsymbol{n} = \boldsymbol{0} & \text{on } \Gamma\,.\end{cases} \tag{109}$$

An additional condition for $\boldsymbol{P}_t(\boldsymbol{x},\boldsymbol{y})$ and $\boldsymbol{C}_t(\boldsymbol{x},\boldsymbol{y})$ is needed to ensure uniqueness, such as the following:

$$\langle\boldsymbol{P}_t(\boldsymbol{x},\boldsymbol{y})\rangle_t = \boldsymbol{0} \quad \text{and} \quad \langle\boldsymbol{C}_t(\boldsymbol{x},\boldsymbol{y})\rangle_t = \boldsymbol{0}. \tag{110}$$

Then, a cell averaging of Equation (85) over Ω_t provides the following:

$$\begin{aligned}\left\langle\boldsymbol{u}_t^{(0)}\right\rangle_t = &-\overline{\kappa}\left\langle\overline{\mathsf{A}}\right\rangle_t\nabla_{\boldsymbol{x}}p_t^{(0)} + \overline{\kappa}\left\langle\overline{\mathsf{A}}\left(\nabla_{\boldsymbol{y}}\boldsymbol{P}_t\right)^{\mathrm{T}}\right\rangle_t\nabla_{\boldsymbol{x}}p_t^{(0)}\\ &+\overline{\kappa}\left\langle\overline{\mathsf{A}}\left(\nabla_{\boldsymbol{y}}\boldsymbol{C}_t\right)^{\mathrm{T}}\right\rangle_t\nabla_{\boldsymbol{x}}c_t^{(0)} \quad \text{in } \Omega_t\,.\end{aligned} \tag{111}$$

Finally, defining the tensors

$$\mathsf{F} = \overline{\kappa}\left\langle\overline{\mathsf{A}} - \overline{\mathsf{A}}\left(\nabla_{\boldsymbol{y}}\boldsymbol{P}_t\right)^{\mathrm{T}}\right\rangle_t \tag{112}$$

and

$$\mathsf{G} = \overline{\kappa}\left\langle\overline{\mathsf{A}}\left(\nabla_{\boldsymbol{y}}\boldsymbol{C}_t\right)^{\mathrm{T}}\right\rangle_t, \tag{113}$$

we obtain a macroscale equation for the average velocity in tumor micro-environment as follows:

$$\left\langle\boldsymbol{u}_t^{(0)}\right\rangle_t = -\mathsf{F}\nabla_{\boldsymbol{x}}p_t^{(0)} + \mathsf{G}\nabla_{\boldsymbol{x}}c_t^{(0)} \quad \text{in } \Omega_t, \tag{114}$$

The average velocity profile in the tumor micro-environment is given by the sum of two distinct contributions. The first term on the r.h.s. of (114) states that the flux is proportional to the gradient of the leading-order pressure, $p_t^{(0)}$, and it can thus be seen as an anisotropic Darcy's law at the macroscale. The second term

on the r.h.s. of (114) accounts for cell motion driven by the gradient of the leading-order chemical concentration $c_t^{(0)}$, resembling a generalization of the Keller–Segel chemotactic velocity at the macroscale.

The influence of the microstructure is incorporated through the tensors F and G, respectively.

To close the entire macroscale model, we need a macroscale equation for the leading order pressure $p_t^{(0)}$. To obtain it, we collect the ε^2 coefficients in (42) and the ε^1 coefficients in (47) as follows:

$$\begin{aligned}
&\nabla_{\boldsymbol{x}} \cdot \boldsymbol{u}_t^{(0)} + \nabla_{\boldsymbol{y}} \cdot \boldsymbol{u}_t^{(1)} \\
&= \overline{\gamma} c_t^{(0)} + \nabla_{\boldsymbol{x}} \cdot \left(\overline{\chi}(\boldsymbol{x}, \boldsymbol{y}) \overline{\mathsf{A}}(\boldsymbol{x}, \boldsymbol{y}) \nabla_{\boldsymbol{x}} c_t^{(0)} \right) \\
&\quad + \nabla_{\boldsymbol{x}} \cdot \left(\overline{\chi}(\boldsymbol{x}, \boldsymbol{y}) \overline{\mathsf{A}}(\boldsymbol{x}, \boldsymbol{y}) \nabla_{\boldsymbol{y}} c_t^{(1)} \right) \\
&\quad + \nabla_{\boldsymbol{y}} \cdot \left(\overline{\chi}(\boldsymbol{x}, \boldsymbol{y}) \overline{\mathsf{A}}(\boldsymbol{x}, \boldsymbol{y}) \nabla_{\boldsymbol{x}} c_t^{(1)} \right) \\
&\quad + \nabla_{\boldsymbol{y}} \cdot \left(\overline{\chi}(\boldsymbol{x}, \boldsymbol{y}) \overline{\mathsf{A}}(\boldsymbol{x}, \boldsymbol{y}) \nabla_{\boldsymbol{y}} c_t^{(2)} \right) \quad \text{in } \Omega_t \,,
\end{aligned} \tag{115}$$

$$\boldsymbol{u}_t^{(1)} \cdot \boldsymbol{n}_t = -\overline{\mathcal{J}}_b^{(0)} \quad \text{on } \Gamma, \tag{116}$$

where we recall that $\boldsymbol{n}_t = -\boldsymbol{n}$.

An integral averaging of the first equation over Ω_t, using the divergence theorem in the $\boldsymbol{y}$ variable, provides the following:

$$\begin{aligned}
\nabla_{\boldsymbol{x}} \cdot \left\langle \boldsymbol{u}_t^{(0)} \right\rangle_t + \frac{1}{|\Omega_t|} \int_\Gamma \boldsymbol{u}_t^{(1)} \cdot \boldsymbol{n}_t \, dS_{\boldsymbol{y}} &= \overline{\gamma} c_t^{(0)} + \nabla_{\boldsymbol{x}} \cdot \left(\left\langle \overline{\chi} \overline{\mathsf{A}} \right\rangle_t \nabla_{\boldsymbol{x}} c_t^{(0)} \right) \\
&\quad - \nabla_{\boldsymbol{x}} \cdot \left(\left\langle \overline{\chi} \overline{\mathsf{A}} (\nabla_{\boldsymbol{y}} \boldsymbol{b})^{\mathrm{T}} \right\rangle_t \nabla_{\boldsymbol{x}} c_t^{(0)} \right) \\
&\quad + \frac{1}{|\Omega_t|} \int_\Gamma \overline{\chi} \left(\overline{\mathsf{A}} \nabla_{\boldsymbol{x}} c_t^{(1)} + \overline{\mathsf{A}} \nabla_{\boldsymbol{y}} c_t^{(2)} \right) \cdot \boldsymbol{n}_t \, dS_{\boldsymbol{y}} \quad \text{in } \Omega_t \,.
\end{aligned} \tag{117}$$

Taking into account the interface conditions (87) and (116), we can rewrite the interface condition (101) as follows:

$$\left(\overline{\mathsf{A}} \nabla_{\boldsymbol{x}} c_t^{(1)} + \overline{\mathsf{A}} \nabla_{\boldsymbol{y}} c_t^{(2)} \right) \cdot \boldsymbol{n}_t = -\frac{\overline{\mathcal{J}}_b^{(0)}}{\overline{D}_t} c_t^{(0)} + \frac{\overline{\mathcal{J}}_d^{(0)}}{\overline{D}_t} \quad \text{on } \Gamma, \tag{118}$$

Using the interface conditions (116) and (118) and defining $\mathsf{C} = \left\langle \overline{\chi} \overline{\mathsf{A}} - \overline{\chi} \overline{\mathsf{A}} (\nabla_{\boldsymbol{y}} \boldsymbol{b})^{\mathrm{T}} \right\rangle_t$, we can rewrite Equation (117) as follows:

$$\begin{aligned}
&\nabla_{\boldsymbol{x}} \cdot \left\langle \boldsymbol{u}_t^{(0)} \right\rangle_t \\
&= \overline{\gamma} c_t^{(0)} + \frac{1}{|\Omega_t|} \int_\Gamma \overline{\mathcal{J}}_b^{(0)} \, dS_{\boldsymbol{y}} + \frac{1}{|\Omega_t|} \int_\Gamma \overline{\chi}(\boldsymbol{x}, \boldsymbol{y}) \frac{\overline{\mathcal{J}}_d^{(0)}}{\overline{D}_t} \, dS_{\boldsymbol{y}} \\
&\quad - \frac{1}{|\Omega_t|} \int_\Gamma \overline{\chi}(\boldsymbol{x}, \boldsymbol{y}) \frac{\overline{\mathcal{J}}_b^{(0)}}{\overline{D}_t} c_t^{(0)} \, dS_{\boldsymbol{y}} + \nabla_{\boldsymbol{x}} \cdot \left(\mathsf{C} \nabla_{\boldsymbol{x}} c_t^{(0)} \right) \quad \text{in } \Omega_t \,.
\end{aligned} \tag{119}$$

Next, we observe that the fluxes $\overline{\mathcal{J}}_b^{(0)}$ and $\overline{\mathcal{J}}_d^{(0)}$, as defined in Equations (67–80), are independent of $\boldsymbol{y}$ due to the conditions specified in (51), (70), (84), and (92). Consequently, we obtain the following:

$$\begin{aligned}
\nabla_{\boldsymbol{x}} \cdot \left\langle \boldsymbol{u}_t^{(0)} \right\rangle_t &= \overline{\gamma} c_t^{(0)} + \frac{|\Gamma|}{|\Omega_t|} \overline{\mathcal{J}}_b^{(0)} + \frac{1}{|\Omega_t|} \frac{\overline{\mathcal{J}}_d^{(0)}}{\overline{D}_t} \int_\Gamma \overline{\chi}(\boldsymbol{x}, \boldsymbol{y}) \, dS_{\boldsymbol{y}} \\
&\quad - \frac{1}{|\Omega_t|} \frac{\overline{\mathcal{J}}_b^{(0)}}{\overline{D}_t} c_t^{(0)} \int_\Gamma \overline{\chi}(\boldsymbol{x}, \boldsymbol{y}) \, dS_{\boldsymbol{y}} + \nabla_{\boldsymbol{x}} \cdot \left(\mathsf{C} \nabla_{\boldsymbol{x}} c_t^{(0)} \right) \quad \text{in } \Omega_t \,.
\end{aligned} \tag{120}$$

Finally, we define $X(\boldsymbol{x}) = \int_\Gamma \overline{\chi}(\boldsymbol{x}, \boldsymbol{y}) \, dS_{\boldsymbol{y}}$, and we use Equation (114) to obtain the following:

$$\begin{aligned}
\nabla_{\boldsymbol{x}} \cdot \left(\mathsf{F} \nabla_{\boldsymbol{x}} p_t^{(0)} \right) &= -\overline{\gamma} c_t^{(0)} + \frac{|\Gamma|}{|\Omega_t|} \overline{\mathcal{J}}_b^{(0)} - \frac{1}{|\Omega_t|} \frac{\overline{\mathcal{J}}_d^{(0)}}{\overline{D}_t} X(\boldsymbol{x}) \\
&\quad + \frac{1}{|\Omega_t|} \frac{\overline{\mathcal{J}}_b^{(0)}}{\overline{D}_t} c_t^{(0)} X(\boldsymbol{x}) + \nabla_{\boldsymbol{x}} \cdot \left[(\mathsf{G} - \mathsf{C}) \nabla_{\boldsymbol{x}} c_t^{(0)} \right] \quad \text{in } \Omega_t \,.
\end{aligned} \tag{121}$$

In this case, the effective source term on the right-hand side of Equation (121) primarily arises from the leading-order fluid and nutrient fluxes, $\overline{\mathcal{J}}_b^{(0)}$ and $\overline{\mathcal{J}}_d^{(0)}$. Additionally, there is a further contribution from the gradient of the nutrient concentration.

The differential problem for tumor micro-environment is finally given by Equations (114), (121), and (104) for the tumor micro-environment variables $\left\langle \boldsymbol{u}_t^{(0)} \right\rangle_t$, $p_t^{(0)}$ and $c_t^{(0)}$.

4.2.1 | Particular Case

A particular case arises when the parameter $\overline{\chi}$ is independent both of $\boldsymbol{x}$ and of $\boldsymbol{y}$, that is, $\overline{\chi}(\boldsymbol{x}, \boldsymbol{y}) \equiv \overline{\chi}$. In this specific scenario, we observe a simplification of the tumor micro-environment problem. In fact, Equation (95) can be rewritten as follows:

$$\left(\overline{\chi} c_t^{(0)} - \overline{D}_t \right) \nabla_{\boldsymbol{y}} \cdot \left(\overline{\mathsf{A}}(\boldsymbol{x}, \boldsymbol{y}) \nabla_{\boldsymbol{y}} c_t^{(1)} + \overline{\mathsf{A}}(\boldsymbol{x}, \boldsymbol{y}) \nabla_{\boldsymbol{x}} c_t^{(0)} \right) = 0 \quad \text{in } \Omega_t, \tag{122}$$

One solution of Equation (122) could be

$$c_t^{(0)}(\boldsymbol{x}, t) \equiv \frac{\overline{D}_t}{\overline{\chi}} \,, \quad \forall t \,, \ \forall \boldsymbol{x} \in \Omega_t, \tag{123}$$

Assume that the solution, Equation (122), is trivially satisfied and is valid for any $c_t^{(1)}$. Therefore, without loss of generality, we can state the following ansatz:

$$c_t^{(1)}(\boldsymbol{x}, \boldsymbol{y}, t) = -\boldsymbol{b}(\boldsymbol{x}, \boldsymbol{y}) \cdot \nabla_{\boldsymbol{x}} c_t^{(0)}(\boldsymbol{x}, t) + \tilde{c}_t(\boldsymbol{x}, t). \tag{124}$$

The above ansatz is valid both when $c_t^{(0)}(\boldsymbol{x}, t) = \frac{\overline{D}_t}{\overline{\chi}}$, since (122) is trivially satisfied for any $c_t^{(1)}$, and in this specific case $c_t^{(1)} \equiv \tilde{c}_t(\boldsymbol{x}, t)$ is $\boldsymbol{y}$-independent. It is also valid when $c_t^{(0)}(\boldsymbol{x}, t) \neq \frac{\overline{D}_t}{\overline{\chi}}$, in which case Equation (122) can be rewritten as follows:

$$\nabla_{\boldsymbol{y}} \cdot \left(\overline{\mathsf{A}}(\boldsymbol{x}, \boldsymbol{y}) \nabla_{\boldsymbol{x}} c_t^{(0)} + \overline{\mathsf{A}}(\boldsymbol{x}, \boldsymbol{y}) \nabla_{\boldsymbol{y}} c_t^{(1)} \right) = 0 \quad \text{in } \Omega_t, \tag{125}$$

In the second scenario, in order to find the correct vector $\boldsymbol{b}(\boldsymbol{x}, \boldsymbol{y})$, we insert the ansatz in (125), and we obtain the following cell problem:

$$\begin{cases} \nabla_{\boldsymbol{y}} \cdot \left[(\nabla_{\boldsymbol{y}} \boldsymbol{b}) \mathsf{A}^{\mathrm{T}} \right] = \nabla_{\boldsymbol{y}} \cdot \mathsf{A}^{\mathrm{T}} & \text{in } \Omega_t \,, \\ (\nabla_{\boldsymbol{y}} \boldsymbol{b}) \mathsf{A}^{\mathrm{T}} \boldsymbol{n} = \mathsf{A}^{\mathrm{T}} \boldsymbol{n} & \text{on } \Gamma \,. \end{cases} \tag{126}$$

A further condition for $\boldsymbol{b}$ is required to ensure uniqueness, for example,

$$\langle \boldsymbol{b}(\boldsymbol{x},\boldsymbol{y})\rangle_t = \boldsymbol{0}. \tag{127}$$

Next, our goal is to derive a macroscale equation for the leading-order concentration $c_t^{(0)}$ in Ω_t. To do this, with analogous steps as the general case, we obtain Equation (104). The main difference in this equation lies in the distinct and easier cell problem that the auxiliary vector $\boldsymbol{b}(\boldsymbol{x},\boldsymbol{y})$ must satisfy. In fact, the cell problem (126) is independent of $c_t^{(0)}(\boldsymbol{x},t)$ and, therefore, can be solved once at the outset.

We have now to write an equation for the leading order velocity $\boldsymbol{u}_t^{(0)}$ and pressure $p_t^{(0)}$. Examining Equations (88) and (89), we can now reformulate these expressions, taking into account that $c_t^{(0)}$ is, in any case, independent of $\boldsymbol{y}$. Furthermore, we can either consider the alternative solution (123), which entails that $c_t^{(0)}$ is a global constant and $c_t^{(1)}$ is a $\boldsymbol{y}$-constant function or utilize Equation (125) to obtain the following:

$$\nabla_{\boldsymbol{y}}\cdot\left(\overline{\mathsf{A}}(\boldsymbol{x},\boldsymbol{y})\nabla_{\boldsymbol{y}}p_t^{(1)}\right) = -\nabla_{\boldsymbol{y}}\cdot\left(\overline{\mathsf{A}}(\boldsymbol{x},\boldsymbol{y})\nabla_{\boldsymbol{x}}p_t^{(0)}\right) \quad \text{in } \Omega_t, \tag{128}$$

$$\overline{\mathsf{A}}(\boldsymbol{x},\boldsymbol{y})\nabla_{\boldsymbol{y}}p_t^{(1)}\cdot\boldsymbol{n}_t = -\overline{\mathsf{A}}(\boldsymbol{x},\boldsymbol{y})\nabla_{\boldsymbol{x}}p_t^{(0)}\cdot\boldsymbol{n}_t \quad \text{on } \Gamma. \tag{129}$$

At this point, we can state the following ansatz:

$$p_t^{(1)}(\boldsymbol{x},\boldsymbol{y},t) = -\boldsymbol{P}_t(\boldsymbol{x},\boldsymbol{y})\cdot\nabla_{\boldsymbol{x}}p_t^{(0)}(\boldsymbol{x},t) + \tilde{p}_t(\boldsymbol{x},t), \tag{130}$$

where $\tilde{p}_t(\boldsymbol{x},t)$ denotes the component that is independent of $\boldsymbol{y}$ and the auxiliary vector $\boldsymbol{P}_t(\boldsymbol{x},\boldsymbol{y})$ solve the cell problem:

$$\begin{cases} \nabla_{\boldsymbol{y}}\cdot\left[(\nabla_{\boldsymbol{y}}\boldsymbol{P}_t)\mathsf{A}^{\mathrm{T}}\right] = \nabla_{\boldsymbol{y}}\cdot\mathsf{A}^{\mathrm{T}} & \text{in } \Omega_t, \\ (\nabla_{\boldsymbol{y}}\boldsymbol{P}_t)\mathsf{A}^{\mathrm{T}}\boldsymbol{n} = \mathsf{A}^{\mathrm{T}}\boldsymbol{n} & \text{on } \Gamma. \end{cases} \tag{131}$$

A further condition for $\boldsymbol{P}_t$ is required to ensure uniqueness, for example:

$$\langle \boldsymbol{P}_t(\boldsymbol{x},\boldsymbol{y})\rangle_t = \boldsymbol{0}. \tag{132}$$

Then, an integral averaging of Equation (85) over Ω_t provides the macroscale equation for the velocity in the tumor microenvironment:

$$\left\langle \boldsymbol{u}_t^{(0)}\right\rangle_t = -\overline{\kappa}\left\langle\overline{\mathsf{A}}\right\rangle_t\nabla_{\boldsymbol{x}}p_t^{(0)} - \overline{\kappa}\left\langle\overline{\mathsf{A}}\left(\nabla_{\boldsymbol{y}}\boldsymbol{P}_t\right)^{\mathrm{T}}\right\rangle_t\nabla_{\boldsymbol{x}}p_t^{(0)} \quad \text{in } \Omega_t. \tag{133}$$

Defining $\mathsf{F} = \overline{\kappa}\left\langle\overline{\mathsf{A}} - \overline{\mathsf{A}}\left(\nabla_{\boldsymbol{y}}\boldsymbol{P}_t\right)^{\mathrm{T}}\right\rangle_t$, we obtain a macroscale equation for the average velocity in tumor microenvironment:

$$\left\langle \boldsymbol{u}_t^{(0)}\right\rangle_t = -\mathsf{F}\nabla_{\boldsymbol{x}}p_t^{(0)} \quad \text{in } \Omega_t. \tag{134}$$

In this particular case, in the tumor micro-environment compartment, the average velocity profile is given by an anisotropic Darcy's law. The role of the microstructure is encoded in the permeability tensor, which is given by F. In this formulation, the term representing cell movement driven by the gradient of the leading-order chemical concentration $c_t^{(0)}$, which would otherwise represent the macroscale chemotactic velocity similar to the Keller–Segel model, is absent.

To close the entire macroscale model, we need a macroscale equation for the leading order pressure $p_t^{(0)}$. To derive this result, we gather the ε^2 terms from (42) and the ε^1 terms from (47). By following similar steps as in (117) and subsequent equations and defining $\mathsf{C} = \overline{\chi}\left\langle\overline{\mathsf{A}} - \overline{\mathsf{A}}\left(\nabla_{\boldsymbol{y}}\boldsymbol{b}\right)^{\mathrm{T}}\right\rangle_t$, we obtain the following:

$$\begin{aligned}\nabla_{\boldsymbol{x}}\cdot\left(\mathsf{F}\nabla_{\boldsymbol{x}}p_t^{(0)}\right) = &-\overline{\gamma}c_t^{(0)} - \frac{|\Gamma|}{|\Omega_t|}\overline{\mathcal{J}}_b^{(0)} - \overline{\chi}\frac{|\Gamma|}{|\Omega_t|}\frac{\overline{\mathcal{J}}_d^{(0)}}{\overline{D}_t} \\ &+ \overline{\chi}\frac{|\Gamma|}{|\Omega_t|}\frac{\overline{\mathcal{J}}_b^{(0)}}{\overline{D}_t}c_t^{(0)} - \nabla_{\boldsymbol{x}}\cdot\left[\mathsf{C}\nabla_{\boldsymbol{x}}c_t^{(0)}\right] \quad \text{in } \Omega_t.\end{aligned} \tag{135}$$

Also, in this particular case, the effective source term on the right-hand side primarily arises from the leading-order fluid and nutrient fluxes, $\overline{\mathcal{J}}_b^{(0)}$ and $\overline{\mathcal{J}}_d^{(0)}$, and a further contribution from the gradient of the nutrient concentration.

The differential problem in this particular case is defined by (134), (135), and (104) for the variables $\left\langle \boldsymbol{u}_t^{(0)}\right\rangle_t$, $p_t^{(0)}$, and $c_t^{(0)}$.

Remark 1. We would like to highlight that the particular case can be directly derived from the general case by assuming a constant value for $\overline{\chi}$. Since G is defined by (113) in terms of the auxiliary vector $\boldsymbol{C}_t$, we notice that problem (109), when $\overline{\chi}$ is a constant, reduces to the following:

$$\begin{cases} \nabla_{\boldsymbol{y}}\cdot\left[\overline{\kappa}\left(\nabla_{\boldsymbol{y}}\boldsymbol{C}_t\right)\overline{\mathsf{A}}^{\mathrm{T}}\right] = \overline{\chi}\nabla_{\boldsymbol{y}}\cdot\left[\overline{\mathsf{A}}^{\mathrm{T}} - \left(\nabla_{\boldsymbol{y}}\boldsymbol{b}\right)\overline{\mathsf{A}}^{\mathrm{T}}\right] & \text{in } \Omega_t, \\ \left(\nabla_{\boldsymbol{y}}\boldsymbol{C}_t\right)\overline{\mathsf{A}}^{\mathrm{T}}\boldsymbol{n} = \boldsymbol{0} & \text{on } \Gamma. \end{cases} \tag{136}$$

In this system, the right-hand side equals zero as it corresponds to the first equation of (98) in the case of a constant $\overline{\chi}$. Consequently, the solution to system (136) implies that the vector $\boldsymbol{C}_t$ is constant with respect to $\boldsymbol{y}$. Based on the definition of G in (113), it follows that G is the null tensor, and therefore, it does not appear in (134). As such, the contribution to the modified Darcy's law which is proportional to the gradient of the concentration is directly related to spatial variations of the chemotactic coefficient. However, even when the chemotactic coefficient is a constant, the final model still features additional contributions mediated by the chemotactic coefficient to both the drug and blood fluxes at the macroscale, as per equation (135).

5 | Conclusions

In this paper, we have analyzed a system of partial differential equations (PDEs) in nondimensional form, defined over two distinct domains, Ω_t and Ω_v, governed by the balance laws (21–26). The interaction between these domains is described through the interface conditions (27–29). The model is derived with a focus on a specific application: the description of flow exchange and motion in a tumor microenvironment. Therefore, Ω_t represents the tumor region, while Ω_v corresponds to the capillary network. In this context, net growth may occur, either as a volumetric term or as a mass flux associated with chemotactic accretion. The interface conditions account for the exchange of blood and nutrients across the capillary walls. With slight modifications,

the model could also be adapted to describe a healthy tissue microenvironment or even other scenarios, such as the exchange of substances between roots and soil [35]. By leveraging the separation of scales between the macroscale and microscale, we employed homogenization techniques under the assumptions of local periodicity and macroscopic uniformity to derive a closed system of differential equations for the leading-order quantities: $\left\langle \boldsymbol{u}_t^{(0)} \right\rangle_t$, $\left\langle \boldsymbol{u}_v^{(0)} \right\rangle_v$, $p_t^{(0)}$, $p_v^{(0)}$, $c_t^{(0)}$, and $c_v^{(0)}$.

The resulting system of equations describes fluid flow using a porous medium model. In the tumor microenvironment, the mass balance equation at the macroscopic scale accounts for effective transport between the compartments Ω_t and Ω_v through mass source terms that encapsulate macroscopic changes in the microvasculature. Additionally, a significant novelty with respect to previous models [24, 25] is the inclusion of a macroscopic form of the nonconvective mass flux related to chemotactic growth. In this framework, the average velocity $\left\langle \boldsymbol{u}_t^{(0)} \right\rangle_t$, describing the flow of the biological material, modeled as a fluid, is driven by both the pressure gradient and the nutrient concentration gradient. In contrast, within the capillary domain Ω_v, the fluid flow adheres to classical Darcy's law. The permeability tensors involved in these relations can be computed by solving differential cell problems.

The effective governing equations for nutrients transport are formulated as a coupled advection–diffusion–reaction model. The reaction terms in this model account for nutrient exchange between the two compartments and also reflect the influence of microvascular geometry. The role of the microstructure is also encoded in the effective diffusivity tensors; in Ω_v, these tensors can be computed by solving classical differential problems on a representative unit cell. In contrast, a more complex cell problem, incorporating macroscopic quantities, is necessary for Ω_t.

The primary contribution of this work is the derivation of a mathematical model that captures the key physical phenomena driving tumor growth and fluid flow at the tissue scale. The influence of the microvasculature is integrated through effective macroscale coefficients, which are obtained by solving associated cell problems. Our model represents an initial effort to incorporate the effects of the microstructural characteristics of capillary network into tumor growth simulations, accounting for both volumetric growth and cell mass flux driven by chemotactic processes. Additionally, the model captures the local anisotropy of the microenvironment, which fundamentally affects fluid flow, nutrients transport and diffusion, cell dynamics, and chemotactic accretion in highly anisotropic tissue [71], such as brain [17, 51] and cartilage [72, 73]. However, in its current form, the tumor domain does not evolve over time, a limitation that should be addressed in future studies by employing, for instance, a level set method to account for domain expansion. Additionally, the tumor tissue is represented as an ensemble of cells and liquid, macroscopically modeled as a simple Newtonian fluid, without differentiating between the liquid and cellular components. This assumption limits the ability to fully capture the proliferative nature of tumor growth, suggesting that this aspect should be refined in future work. Furthermore, while mechanical deformations are neglected in the present formulation, extension of this work should consider the poro-mechanical response that typically characterizes tumors [17, 26, 74]. Finally, we remark that all tensors in the model are assumed to scale with the same preferential direction tensor $\mathsf{A}(\boldsymbol{x})$. Relaxing this assumption could represent an interesting development, although it would substantially increase the mathematical complexity of the formulation.

This study lays the groundwork for understanding the impact of vascular geometry and nutrient delivery on tumor growth and its response to chemicals. The proposed mathematical framework can be adapted for numerical simulations of fluid and nutrient transport in realistic tumor geometries reconstructed from medical imaging data. These numerical results can then be validated against clinical observations, and in the long term, the model's predictions could contribute to improving anticancer treatment strategies and support rapidly emerging sophisticated attempts to couple mathematical modeling and machine learning; see, for example, [75].

Author Contributions

Francesca Ballatore: formal analysis, conceptualization, investigation, methodology, writing – original draft, writing-review and editing. **Chiara Giverso:** conceptualization, investigation, methodology, writing – review and editing, supervision. **Raimondo Penta:** conceptualization, investigation, methodology, writing-review and editing, supervision. All authors gave final approval for publication and agreed to be held accountable for the work performed therein.

Acknowledgments

F.B, C.G., and R.P. conducted the research according to the inspiring scientific principles of the National Italian Mathematics Association Indam ("Istituto nazionale di Alta Matematica"), GNFM group. R.P. is partially supported by EPSRC, UK grants EP/S030875/1 and EP/T017899/1. F.B. acknowledges support from the PNRR M4C2 through the project "Made in Italy Circolare e Sostenibile (MICS)," CUP: E13C22001900001.

Conflicts of Interest

The authors declare no conflicts of interest.

Data Availability Statement

This paper is purely theoretical and therefore has no data.

References

1. G. Papanicolau, A. Bensoussan, and J. L. Lions, *Asymptotic Analysis for Periodic Structures* (Elsevier, 1978).

2. N. S. Bakhvalov and G. Panasenko, *Homogenisation: Averaging Processes in Periodic Media: Mathematical Problems in the Mechanics of Composite Materials*, vol. 36 (The Netherlands: Springer Science & Business Media, 1989).

3. C. C. Mei and B. Vernescu, *Homogenization Methods for Multiscale Mechanics* (Singapore: World scientific, 2010).

4. D. Cioranescu and P. Donato, *An Introduction to Homogenization. 17* (Oxford: Oxford University Press, 1999).

5. R. Penta, A. Gerisch. An Introduction to Asymptotic Homogenization. In: Springer. 2017:1–26.

6. R. Penta and A. Gerisch, "Investigation of the Potential of Asymptotic Homogenization for Elastic Composites via a Three-Dimensional Computational Study," *Computing and Visualization in Science* 17 (2015): 185–201.

7. R. Penta and A. Gerisch, "The Asymptotic Homogenization Elasticity Tensor Properties for Composites With Material Discontinuities," *Continuum Mechanics and Thermodynamics* 29 (2017): 187–206.

8. C. Soyarslan, J. Havinga, L. Abelmann, and T. Van den Boogaard, "Asymptotic Homogenization in the Determination of Effective Intrinsic Magnetic Properties of Composites," *Results in Physics* 44 (2023): 106188.

9. F. Fantoni, A. Bacigalupo, and M. Paggi, "Multi-Field Asymptotic Homogenization of Thermo-Piezoelectric Materials With Periodic Microstructure," *International Journal of Solids and Structures* 120 (2017): 31–56.

10. B. E. Abali and E. Barchiesi, "Additive Manufacturing Introduced Substructure and Computational Determination of Metamaterials Parameters by Means of the Asymptotic Homogenization," *Continuum Mechanics and Thermodynamics* 33, no. 4 (2021): 993–1009.

11. U. Hornung, *Homogenization and Porous Media. 6* (Springer Science & Business Media, 1997).

12. D. Łydżba, *Micromechanical Analysis of Saturated Porous Media With Local Mass Exchange Phenomenon* (Springer, 2005), 57–81.

13. T. Arbogast and H. Lehr, "Homogenization of a Darcy-Stokes System Modeling Vuggy Porous Media," *Computational Geosciences* 10 (2006): 291–302.

14. M. P. Dalwadi, M. Bruna, and I. M. Griffiths, "A Multiscale Method to Calculate Filter Blockage," *Journal of Fluid Mechanics* 809 (2016): 264–289.

15. R. Penta, K. Raum, Q. Grimal, S. Schrof, and A. Gerisch, "Can a Continuous Mineral Foam Explain the Stiffening of Aged Bone Tissue? A Micromechanical Approach to Mineral Fusion in Musculoskeletal Tissues," *Bioinspiration & Biomimetics* 11, no. 3 (2016): 035004.

16. S. Dumont, M. Serpilli, R. Rizzoni, and F. C. Lebon, "Numerical Validation of Multiphysic Imperfect Interfaces Models," *Frontiers in Materials* 7 (2020): 158.

17. H. Dehghani, I. Noll, R. Penta, A. Menzel, and J. Merodio, "The Role of Microscale Solid Matrix Compressibility on the Mechanical Behaviour of Poroelastic Materials," *European Journal of Mechanics - A/Solids* 83 (2020): 103996.

18. L. Miller and R. Penta, "Investigating the Effects of Microstructural Changes Induced by Myocardial Infarction on the Elastic Parameters of the Heart," *Biomechanics and Modeling in Mechanobiology* 22, no. 3 (2023): 1019–1033.

19. T. Roose and M. A. Swartz, "Multiscale Modeling of Lymphatic Drainage From Tissues Using Homogenization Theory," *Journal of Biomechanics* 45, no. 1 (2012): 107–115.

20. A. Girelli, G. Giantesio, A. Musesti, and R. Penta, "Effective Governing Equations for Dual Porosity Darcy–Brinkman Systems Subjected to Inhomogeneous Body Forces and Their Application to the Lymph Node," *Proceedings of the Royal Society A* 479, no. 2276 (2023): 20230137.

21. R. D. O'Dea, M. Nelson, A. El Haj, S. L. Waters, and H. M. Byrne, "A Multiscale Analysis of Nutrient Transport and Biological Tissue Growth In Vitro," *Mathematical Medicine and Biology: A Journal of the IMA.* 32, no. 3 (2015): 345–366.

22. A. Ramírez-Torres, R. Rodríguez-Ramos, F. J. Sabina, et al., "The Role of Malignant Tissue on the Thermal Distribution of Cancerous Breast," *Journal of Theoretical Biology* 426 (2017): 152–161.

23. S. Di Stefano, A. Ramírez-Torres, R. Penta, and A. Grillo, "Self-Influenced Growth Through Evolving Material Inhomogeneities," *International Journal of Non-Linear Mechanics* 106 (2018): 174–187.

24. R. Shipley and S. Chapman, "Multiscale Modelling of Fluid and Drug Transport in Vascular Tumours," *Bulletin of Mathematical Biology* 72 (2010): 1464–1491.

25. R. Penta, D. Ambrosi, and A. Quarteroni, "Multiscale Homogenization for Fluid and Drug Transport in Vascularized Malignant Tissues," *Mathematical Models and Methods in Applied Sciences* 25 (2014): 79–108.

26. R. Penta and J. Merodio, "Homogenized Modeling for Vascularized Poroelastic Materials," *Meccanica* 52 (2017): 3321–3343.

27. A. Ramrez-Torres, S. Di Stefano, A. Grillo, J. Merodio, and R. Penta, "An Asymptotic Homogenization Approach to the Microstructural Evolution of Heterogeneous Media," *International Journal of Non-Linear Mechanics* 106 (2018): 245–257.

28. M. P. Dalwadi, I. M. Griffiths, and M. Bruna, "Understanding How Porosity Gradients Can Make a Better Filter Using Homogenization Theory," *Proceedings of the Royal Society A: Mathematical, Physical and Engineering Science* 471 (2015): 20150464.

29. G. Savio, A. Curtarello, S. Rosso, R. Meneghello, and G. Concheri, "Homogenization Driven Design of Lightweight Structures for Additive Manufacturing," *International Journal on Interactive Design and Manufacturing (IJIDeM)* 13 (2019): 263–276.

30. M. Taffetani, C. De Falco, R. Penta, D. Ambrosi, and P. Ciarletta, "Biomechanical Modelling in Nanomedicine: Multiscale Approaches and Future Challenges," *Archive of Applied Mechanics* 84 (2014): 1627–1645.

31. P. Carmeliet, "Mechanisms of Angiogenesis and Arteriogenesis," *Nature Medicine* 6 (2000): 389–395.

32. T. Koch, K. Heck, N. Schröder, H. Class, and R. Helmig, "A new Simulation Framework for Soil–Root Interaction, Evaporation, Root Growth, and Solute Transport," *Vadose Zone Journal* 17, no. 1 (2018): 1–21.

33. S. Scialò, "A Five Field Formulation for Flow Simulations in Porous Media With Fractures and Barriers via an Optimization Based Domain Decomposition Method," *Finite Elements in Analysis and Design* 238 (2024): 104204.

34. S. Berrone, D. Grappein, S. Scialò, and F. Vicini, "A Gradient Based Resolution Strategy for a PDE-Constrained Optimization Approach for 3D-1D Coupled Problems," *International Journal on Geomathematics* 13 (2022): 1–25.

35. A. W. Mahdiyasa, D. J. Large, M. Icardi, and B. P. Muljadi, "MPeat2D–A Fully Coupled Mechanical-Ecohydrological Model of Peatland Development in Two Dimensions," *EGUsphere.* 2023 (2023): 1–31.

36. J. Less, T. Skalak, E. Sevick, and R. Jain, "Microvascular Architecture in a Mammary Carcinoma: Branching Patterns and Vessel Dimensions," *Cancer Research* 15, no. 1 (1991): 265–273.

37. J. Folkman, "The Vascularization of Tumors," *Scientific American* 234, no. 5 (1976): 58–73.

38. M. Chaplain, "Avascular Growth, Angiogenesis and Vascular Growth in Solid Tumours: The mathematical Modelling of the Stages of Tumour Development," *Mathematical and Computer Modelling* 23, no. 6 (1996): 47–87.

39. D. Ambrosi and L. Preziosi, "On the Closure of Mass Balance Models for Tumor Growth," *Mathematical Models and Methods in Applied Sciences* 12 (2011): 737–754.

40. H. M. Byrne and M. A. J. Chaplain, "Free Boundary Value Problems Associated With the Growth and Development of Multicellular Spheroids," *European Journal of Applied Mathematics* 8, no. 6 (1997): 639–658.

41. C. Giverso and P. Ciarletta, "On the Morphological Stability of Multicellular Tumour Spheroids Growing in Porous Media," *European Physical Journal E, Soft Matter* 39, no. 10 (2016): 92.

42. Z. B. Fülöp, A. Ramírez-Torres, and R. Penta, "Multiscale Modelling of Fluid Transport in Vascular Tumours Subjected to Electrophoresis Anticancer Therapies," *Zeitschrift für Angewandte Mathematik und Physik* 75, no. 1 (2024): 9.

43. L. Cattaneo and P. Zunino, "Computational Models for Fluid Exchange Between Microcirculation and Tissue Interstitium," *Networks and Heterogeneous Media* 9, no. 1 (2014): 135–159.

44. S. Berrone, C. Giverso, D. Grappein, L. Preziosi, and S. Scial, "An Optimization Based 3D-1D Coupling Strategy for Tissue Perfusion and Chemical Transport During Tumor-Induced Angiogenesis," *Computers & Mathematics with Applications* 151 (2023): 252–270.

45. E. F. Keller and L. A. Segel, "Model for Chemotaxis," *Journal of Theoretical Biology* 30, no. 2 (1971): 225–234.

46. T. Hillen and K. J. Painter, "A User's Guide to PDE Models for Chemotaxis," *Journal of Mathematical Biology* 58, no. 1 (2009): 183–217.

47. C. Giverso, M. Verani, and P. Ciarletta, "Emerging Morphologies in Round Bacterial Colonies: Comparing Volumetric Versus Chemotactic Expansion," *Biomechanics and Modeling in Mechanobiology* 15, no. 3 (2016): 643–661.

48. B. Perthame, *Transport Equations in Biology* (Basel: Birkhuser, 2007).

49. S. Childress and J. Percus, "Nonlinear Aspects of cHemotaxis," *Mathematical Biosciences* 56, no. 3 (1981): 217–237.

50. F. Ballatore, G. Lucci, A. Borio, and C. Giverso, "An Imaging-Informed Mechanical Framework to Provide a Quantitative Description of Brain Tumour Growth and the Subsequent Deformation of White Matter Tracts," in *Mathematical models and computer simulations for biomedical applications*, eds. G. Bretti, R. Natalini, P. Palumbo, and L. Preziosi (Springer Series, 2023).

51. F. Ballatore, G. Lucci, and C. Giverso, "Modelling and Simulation of Anisotropic Growth in Brain Tumours Through Poroelasticity: A Study of Ventricular Compression and Therapeutic Protocols," *Computational Mechanics* 74 (2024): 1137–1169.

52. G. Lucci, A. Agosti, P. Ciarletta, and C. Giverso, "Coupling Solid and Fluid Stresses With Brain Tumour Growth and White Matter Tract Deformations in a Neuroimaging-Informed Model," *Biomechanics and Modeling in Mechanobiology* 21 (2022): 1483–1509.

53. P. Basser, "Inferring Microstructural Features and the Physiological State of Tissues From Diffusion-Weighted Images," *NMR in Biomedicine* 8 (1995): 333–344.

54. Y. Assaf and O. Pasternak, "Diffusion Tensor Imaging (DTI)-Based White Matter Mapping in Brain Research: A Review," *Journal of molecular neuroscience : MN* 34 (2008): 51–61.

55. S. Chien, S. Usami, R. J. Dellenback, and M. I. Gregersen, "Shear-Dependent Deformation of Erythrocytes in Rheology of Human Blood," *American Journal of Physiology-Legacy Content* 219, no. 1 (1970): 136–142.

56. E. Nader, S. Skinner, M. Romana, et al., "Blood Rheology: Key Parameters, Impact on Blood Flow, Role in Sickle Cell Disease and Effects of Exercise," *Frontiers in Physiology* 10 (2019): 1329.

57. A. N. Beris, J. S. Horner, S. Jariwala, M. J. Armstrong, and N. J. Wagner, "Recent Advances in Blood Rheology: A Review," *Soft Matter* 17 (2021): 10591–10613.

58. O. Kedem and A. Katchalsky, "Thermodynamic Analysis of the Permeability of Biological Membranes to Non-Electrolytes," *Biochimica et Biophysica Acta* 27 (1958): 229–246.

59. R. K. Jain, R. T. Tong, and L. L. Munn, "Effect of Vascular Normalization by Antiangiogenic Therapy on Interstitial Hypertension, Peritumor Edema, and Lymphatic Metastasis: Insights From a Mathematical Model," *Cancer Research* 67, no. 6 (2007): 2729–2735.

60. M. H. Friedman, *Principles and Models of Biological Transport* (New York, NY: Springer-Verlag, 2008).

61. K. Perktold, M. Prosi, and P. Zunino, *Mathematical Models of Mass Transfer in the Vascular Walls: 243–278* (Milano: Springer Milan, 2009).

62. R. J. Shipley, A. F. Smith, P. W. Sweeney, A. R. Pries, and T. W. Secomb, "A Hybrid Discrete–Continuum Approach for Modelling Microcirculatory Blood Flow," *Mathematical medicine and biology: A journal of the IMA.* 37, no. 1 (2020): 40–57.

63. M. Discacciati and A. Quarteroni, "Navier-Stokes/Darcy Coupling: Modeling, Analysis, and Numerical Approximation," *Revista Matemtica Complutense* 22 (2009): 315–426.

64. G. S. Beavers and D. D. Joseph, "Boundary Conditions at a Naturally Permeable Wall," *Journal of Fluid Mechanics* 30, no. 1 (1967): 197207.

65. I. Jones, "Low Reynolds Number Flow Past a Porous Spherical Shell," *Mathematical Proceedings of the Cambridge Philosophical Society* 73 (1973): 231–238.

66. P. Saffman, "On the Boundary Condition at the Surface of porous medium," *Studies in Applied Mathematics* 50 (1971): 93–101.

67. Y. Cao, M. Gunzburger, F. Hua, and X. Wang, "Coupled Stokes-Darcy Model With Beavers-Joseph Interface Boundary Condition," *Communications in Mathematical Sciences* 8, no. 1 (2010): 1–25.

68. E. Eggenweiler and I. Rybak, "Unsuitability of the Beavers-Joseph Interface Condition for Filtration Problems," *Journal of Fluid Mechanics* 892 (2020): A10.

69. R. Penta, A. Ramirez Torres, J. Merodio, and R. Rodríguez-Ramos, "Effective Governing Equations for Heterogenous Porous Media Subject to Inhomogeneous Body Forces," *Mathematics in Engineering* 3, no. 4 (2021): 1–17.

70. M. H. Holmes, *Introduction to Perturbation Methods. 20* (Springer Science & Business Media, 1995).

71. S. Harmansa, A. Erlich, C. Eloy, G. Zurlo, and T. Lecuit, "Growth Anisotropy of the Extracellular Matrix Shapes a Developing Organ," *Nature Communications* 14, no. 1 (2023): 1220.

72. A. Grillo, A. Guaily, C. Giverso, and S. Federico, "Non-Linear Model for Compression Tests on Articular Cartilage," *Journal of Biomechanical Engineering* 137, no. 7 (2015): 071004.

73. S. Federico, A. Grillo, G. La Rosa, G. Giaquinta, and W. Herzog, "A Transversely Isotropic, Transversely Homogeneous Microstructural-Statistical Model of Articular Cartilage," *Journal of Biomechanics* 38, no. 10 (2005): 2008–2018.

74. D. Ambrosi, S. Pezzuto, D. Riccobelli, T. Stylianopoulos, and P. Ciarletta, "Solid Tumors Are Poroelastic Solids With a Chemo-Mechanical Feedback on Growth," *Journal of Elasticity* 129 (2017): 107–124.

75. P. Mascheroni, S. Savvopoulos, J. C. L. Alfonso, M. Meyer-Hermann, and H. Hatzikirou, "Improving Personalized Tumor Growth Predictions Using a Bayesian Combination of Mechanistic Modeling and Machine Learning," *Communication & Medicine* 1, no. 1 (2021): 19.